



# Performance of multistage-fractured horizontal wells with secondary discrete fractures in heterogeneous tight reservoirs

Qi Deng<sup>1,2</sup> · Jianhua Qu<sup>1,2</sup> · Zhongrong Mi<sup>1,2</sup> · Bing Xu<sup>1,2</sup> · Xindong Lv<sup>1,2,5</sup> · Kai Huang<sup>1,2</sup> · Boning Zhang<sup>1,2</sup> · Ren-Shi Nie<sup>3</sup> · Shengnan Chen<sup>4</sup>

Received: 10 June 2023 / Accepted: 3 January 2024 / Published online: 13 February 2024  
© The Author(s) 2024

## Abstract

A significant portion of tight sandstone reservoirs commonly displays intricate fluvial channels or fault systems. Despite various attempts at analytical/semi-analytical modeling of multistage-fractured horizontal wells (MFHWs) in unconventional reservoirs, the majority of studies have focused on scenarios with homogeneous original physical properties, neglecting cases where MFHWs traverse multiple regions in channelized heterogeneous reservoirs. Comprehending the influence of heterogeneous and leaky faults on the performance of MFHWs is essential for efficient development. This study presents an innovative semi-analytical model to analyze the pressure transient behavior of MFHWs with secondary fractures as they traverse multiple regions in banded channel heterogeneous reservoirs, particularly considering the presence of partially-communicating faults. The approach combines the source method and Green's function method to obtain solutions, introducing a novel technique for discretizing fractures without discretizing interfaces. The effects of the reservoir heterogeneity, partially-communicating faults and fractures system on pressure behavior are analyzed. The results indicate that the pressure behavior of MFHWs passing through regions with different physical properties exhibits distinctive characteristics, differing from both the homogeneous case and the heterogeneous cases where the well does not traverse distinct regions. Permeability heterogeneity influences the curves of all other flow regimes, except the early and late flow regimes. Faults affect transient pressure behavior only when not positioned in the middle of each two primary fractures. Region area heterogeneity primarily influences the medium flow regimes. This work provides valuable insights into the performance of MFHWs in channelized heterogeneous reservoirs, offering technical support for well testing in these reservoirs.

**Keywords** Pressure transient behavior · Multistage-fractured horizontal wells · Secondary fractures · Heterogeneous tight reservoirs · Faults

✉ Qi Deng  
dengqi@zhenhuaoil.com

✉ Jianhua Qu  
qujh@zhenhuaoil.com

<sup>1</sup> Chengdu Northern Petroleum Exploration and Development Technology Co. Ltd, Chengdu 610051, Sichuan Province, People's Republic of China

<sup>2</sup> China Zhenhua Oil Co., Ltd., Beijing 100031, China

<sup>3</sup> State Key Laboratory of Oil and Gas Reservoir Geology and Exploitation, Southwest Petroleum University, Chengdu 610500, Sichuan Province, People's Republic of China

<sup>4</sup> Department of Chemical and Petroleum Engineering, University of Calgary, 2500 University Drive NW, Calgary, Alberta T2N 1N4, Canada

<sup>5</sup> Chengdu University of Technology, Chengdu, 610059, China

## List of symbols

$B$	Volume factor, dimensionless
$C$	Wellbore storage coefficient, $m^3/MPa$
$C_t$	Total compressibility, $MPa^{-1}$
$h$	Reservoir thickness, m
$k$	Reservoir permeability, mD
$k_a$	The permeability of the fault, mD
$L_{PFI}$	The fracture length for the $l$ -th primary fracture, m
$L_{SFI}$	The fracture length for the $l$ -th secondary fracture, m
$M_{PF}$	The number of discrete segments in the primary fractures
$M_{SF}$	The number of discrete segments in the secondary fractures
$N$	The number of regions
$N_{PF}$	The number of primary fractures
$N_{SF}$	The number of secondary fractures

$p$	Pressure, MPa	$x_j$	The distance from the fault $j$ to the original point of the coordinate, m
$p_i$	Initial reservoir pressure, MPa	$x_{w/fj}$	The distance from the fracture $j$ to the original point of the coordinate, m
$\bar{p}_{f_{sj},l,kD}$	The dimensionless Laplace domain solution for a fracture segment in the multi-region composite matrix system	$x_{w/fD}, y_{w/fD}$	The value of starting coordinates of the starting $l$ -th fracture
$\bar{p}_{hfj,l,kD}$	The dimensionless Laplace domain solution for the $k$ -th segment of the $l$ -th fracture in a homogeneous rectangular banded system with the properties of the $j$ -th region	$\hat{x}_{fl}$	The local Cartesian coordinate system associated with the $l$ -th fracture
$\bar{p}_{interSF/D}$	The dimensionless pressure of intersectional segment in the $l$ -th secondary fracture in the Laplace domain.	$\hat{x}_{PFm,l,kD}$	Dimensionless distance of the midpoint of the $k$ -th segment in the $l$ -th primary fracture
$\bar{p}_{interPF/D}$	The dimensionless pressure of intersectional segment in primary fracture connected to the $l$ -th secondary fracture in the Laplace domain	$\hat{x}_{SFm,l,kD}$	Dimensionless distance of the midpoint of the $k$ -th segment in the $l$ -th secondary fracture
$\bar{p}_{jD}$	Dimensionless Laplace domain solution in the multi-region composite matrix system	$\Delta\hat{x}_{PF/D}$	The dimensionless length of each segment of the $l$ -th primary fracture
$\bar{p}_{nsfj,l,kD}$	The dimensionless no-source Laplace domain solution to a rectangular banded linear composite system for the $j$ -th region	$\Delta\hat{x}_{SF/D}$	The dimensionless length of each segment of the $l$ -th secondary fracture
$\bar{p}_{wD}$	The dimensionless wellbore pressure in the Laplace domain	$y_e$	The width of the reservoir, m
$q$	Production rate, m <sup>3</sup> /ks	$\eta$	Diffusivity, m <sup>2</sup> /ks
$q_{fl}$	The flow rate per unit length of the $l$ -th fracture face, m <sup>2</sup> /ks	$\theta_{fl}$	The azimuth between the $l$ -th fracture segment and $x$ axis, radian
$q_{wPFI}$	The flow rate per unit length from the $l$ -th primary fracture to wellbore, m <sup>2</sup> /ks	$\lambda$	Mobility, mD/mPa s
$q_{wSFI}$	The flow rate from the $l$ -th secondary fracture to the primary fracture connected it, m <sup>2</sup> /ks	$\lambda_a$	The mobility of fault, mD/mPa s
$\bar{q}_{interPF/D}$	The dimensionless flow rate caused by the intersectional segment in primary fracture connected to the $l$ -th secondary fracture in the Laplace domain	$\mu$	Fluid viscosity, mPa s
$\bar{q}_{interPF/D}^*$	The total dimensionless flow rate of intersectional segment in primary fracture connected to the $l$ -th secondary fracture in the Laplace domain	$\varphi$	Rock porosity, %
$\bar{q}_{l,kD}$	The dimensionless flow rate from matrix from a fracture segment in Laplace domain	$\chi_{mNFj}$	The inter-porosity flow coefficient in region $j$
$s$	Laplace transform variable based on $t_D$ , dimensionless	$\omega$	Storativity, MPa <sup>-1</sup>
$S$	Skin factor, dimensionless	$\omega_{NFj}$	The storage ratio between naturally fractures and matrix in region $j$
$S_a$	Fault skin, dimensionless		
$t$	Production time, ks		
$w_a$	The half-width of the fault, m		
$w_f$	The width of the $l$ -th fracture, m		
$x, y$	Cartesian coordinates		
$x_e$	The length of the reservoir, m		
$x_{fl,kD}, x_{fl,k+1D}$	The value of starting and ending $x$ coordinates of the $k$ -th segment of the $l$ -th fracture, respectively		

### Superscript

- Laplace domain

### Subscript

D Dimensionless  
 $f$  Primary fracture (PF) or secondary fracture (SF)  
 $j$  The region number,  $j = 1, \dots, N$   
 $k$  Segment of fracture,  $k = 1, \dots, M_{PF}$  for PF and  $k = 1, \dots, M_{SF}$  for SF  
 $l$  Fracture number,  $l = 1, \dots, N_{PF}$  for PF and  $l = 1, \dots, N_{SF}$  for SF  
min The region number with the minimum permeability

### Abbreviations

MFHWs Multistage-fractured horizontal wells  
PF Primary fracture  
SF Secondary fracture  
SRV Stimulated reservoir volume

## Introduction

Unconventional tight oil/gas reservoirs have significantly contributed to the global hydrocarbon supply over the past decade. MFHWs are commonly employed for developing these reservoirs due to their extremely low permeability. It has been postulated that fractures do not have an ideal bi-wing shape but instead exhibit induced secondary fractures during the fracturing process. (Daneshy 2003; Weng et al. 2014; Murillo and Salguero 2016; Xiao et al. 2023). Additionally, a substantial portion of the tight reservoirs displays complex fluvial channels, which are highly heterogeneous and often characterized by laterally discontinuous reservoir units (Cuba et al. 2013; Ramirez et al. 2012; McDowell and Plink-Björklund 2013). Moreover, complex fault distributions are also a common characteristic of tight sandstone reservoirs (Kuchuk and Habashy 1997; Dijk et al. 2020; Cui et al. 2021). Consequently, the MFHWs in these reservoirs may intersect various partial hydrologic barriers (e.g., partially communicating faults), and the properties of the formation and generated secondary fractures may also respond differently at different fracturing stages.

Pressure transient analysis is an effective method for characterizing the properties of both hydraulic fractures and the reservoir matrix. Numerous analytical and semi-analytical models have been previously proposed in the literature to extensively investigate the behavior of MFHWs in unconventional reservoirs. In the early 1990s, several semi-analytical models based on the source method were proposed for MFHWs in homogeneous reservoirs. In these models, fractures were considered as simplified bi-wing uniform flux or infinite-conductivity fractures. (Guo et al. 1994; Horne and Temeng 1995; Wan and Aziz 1999; Raghavan et al. 1997). Subsequently, these semi-analytical models were expanded to simulate a more complex bi-wing fractures system, encompassing fractures with various conductivity, inclined angles, intervals, and lengths, in both infinite and closed box-shaped reservoirs (Zerzar et al. Zerzar and Bettam 2003; Al Rbeawi and Tiab 2012; Jia et al. 2014; Yao et al. 2013; Wang 2014; Ren and Guo 2015).

Analytical models were proposed based on various forms of one-dimensional linear flow concerning MFHWs with stimulated reservoir volume (SRV). Brown et al. (2011) firstly established an analytical tri-linear flow model for MFHWs with SRV. In this model, the MFHWs-reservoir system is divided into three rectangular regions: the finite-conductivity hydraulic fractures region, SRV region, and USRV region, with linear flow assumed in all these regions. Based on Brown's tri-linear flow model, several linear flow models have been developed to capture

a broader range of reservoir/fracture properties, and flow regime sequences, such as five-region model (Stalgorova and Mattar 2013), enhanced five-region model (Deng et al. 2015; Heidari Sureshjani and Clarkson 2015; Tao et al. 2018; Wang et al. 2023), and seven-region model (Zeng et al. 2017, 2018, 2019; Guo et al. 2023). While these linear flow models demonstrate high computing efficiency and have been proven accurate for simulating some simple MFHWs-reservoir systems, they fall short in capturing the intricacies of real fracture networks, including irregular spatial distribution and complex interconnected scenarios of fractures. Additionally, these linear flow models are unable to fully characterize the entire pressure behavior and flow regimes, such as the pseudo-radial regime, of the MFHWs-reservoir system.

Unlike the one-dimensional linear flow modelling method, the source method can explicitly simulate the complex fracture systems and capture the entire pressure behavior and flow regimes of the MFHWs-reservoirs system. Lin and Zhu (2012) and Hwang et al. (2013) established semi-analytical models to investigate the behavior of MFHWs, considering infinite-conductivity secondary fractures. Zhou et al. (2014) introduced a semi-analytical approach that combines numerical fracture solutions with analytical reservoir solutions for transient-behavior analysis. Chen et al. (2016a, 2016b, 2018) developed a semi-analytical model for MFHWs, considering orthogonal finite-conductivity secondary fractures by discretizing the fracture networks into multiple cells. They also analyzed the flow regimes and pressure behaviors of such fracture networks. Jia et al. (2016) and Cheng et al. (2017) introduced semi-analytical models for the transient behaviors of MFHWs with complex secondary fracture networks. In their models, fracture solutions were obtained using the finite-difference method, leading to a significant increase in computation cost. Chen et al. (2019) introduced a semi-analytical method to investigate the transient behaviors in fractured reservoirs, considering discrete natural-fracture and hydraulic-fracture networks simultaneously. In their subsequent work (Chen and Yu 2022), they further developed a discrete semi-analytical model to account for more complex fracture distribution cases, including wellbore-isolating/wellbore-connecting fracture networks, wellbore-isolating/wellbore-connecting fractures, and matrix domains. Several authors have also conducted research on semi-analytical models for MFHWs with simplified SRV by considering the SRV as a circular shape enhanced region (Zhao et al. 2014; Xu et al. 2020), a rectangular enhanced region (Medeiros et al. 2008; Zhao 2012; Zhao et al. 2018; Wu et al. 2020) or an arbitrary shape enhanced region (Zhang and Yang 2021; Chu et al. 2022). These works, employing the source method and boundary element method, primarily focused on continuous homogeneous reservoirs.

While numerous analytical or semi-analytical models have been proposed for MFHWs, they have primarily focused on scenarios where the original physical properties of the reservoir are homogeneous. Few studies have explored models for MFHWs in tight heterogeneous reservoirs characterized by channelized or fault systems with linear discontinuity characteristics.

Wang et al. (2017) introduced a semi-analytical model for MFHWs in banded channel heterogeneous reservoirs using the boundary element method. In their approach, the reservoir was divided into several sub-systems, represented as linear assemblies of distinct homogeneous regions. Flow interactions between these regions were resolved by discretizing the interfaces. However, the model did not account for partially communicating faults, a typical characteristic of such heterogeneous tight reservoirs. Additionally, the model only considered orthogonal bi-wing fracture geometry, limiting its effectiveness in capturing complex fracture systems. Moreover, the semi-analytical solutions were obtained through the boundary element method, necessitating interface discretization and increasing computational demands.

Recently, Deng et al. (2022) presented an analytical solution for fluid flows in rectangular bounded anisotropic multi-region linear composite reservoirs, considering partially communicating faults. However, only the case of vertical fractured wells is investigated.

Considering that horizontal wells in heterogeneous reservoirs may intersect numerous partial hydrologic barriers, Shi et al. (2023) proposed a semi-analytical model for a horizontal well intercepting multiple faults in karst carbonate reservoirs. However, the model did not account for hydraulic

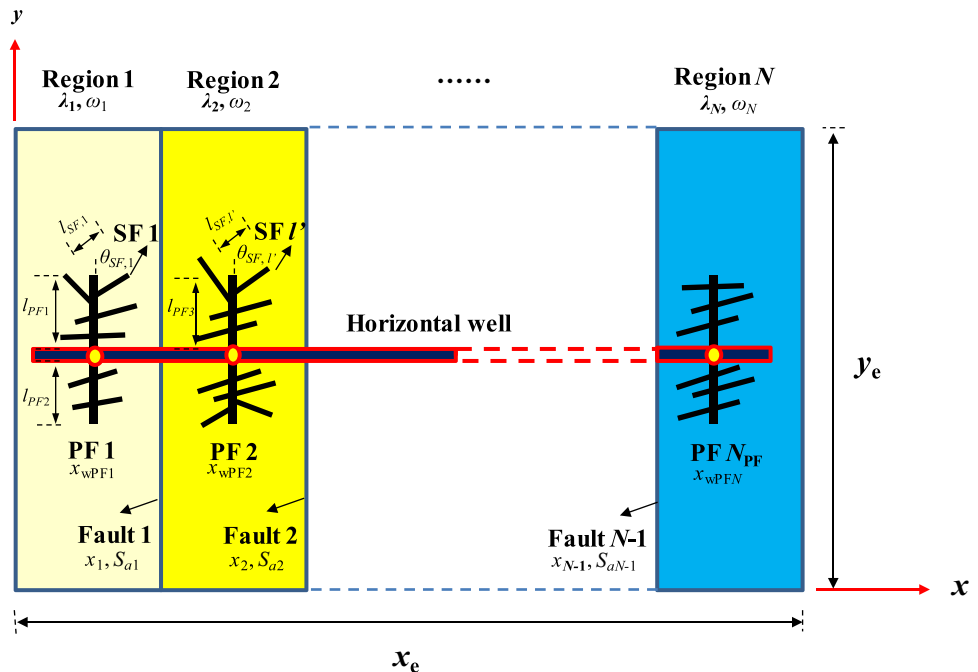
fractures and flow in the matrix, making it specifically suitable for carbonate reservoirs.

To fill this gap, a semi-analytical model is presented for fluid flows to MFHWs with secondary fractures passing through banded channel heterogeneous reservoirs, particularly considering the presence of partially-communicating faults. The reservoir is a multi-region linear composite system that considers different formation properties in each individual region and partially-communicating faults between regions. Secondary discrete fractures can interconnect the primary hydraulic fractures with different inclinations and lengths, while accounting for the effects of wellbore storage and skin. The solution, an extension of our previous analytical solution for fluid flows in a vertically fractured well in bounded multi-region linear composite reservoirs (Deng et al. 2022), is obtained by applying the source method and Green’s function method, eliminating the need for discretizing the interfaces to reduce computational costs. The performance and relative sensitivity of the solution are finally analyzed using type curves.

### Conceptual model

Figure 1 depicts the schematics of the two-dimensional top view of the conceptual model for a multistage-fractured horizontal well with secondary fractures in a banded channel heterogeneous reservoir. The banded channel heterogeneous reservoir is divided into multiple cubical regions along the lateral direction by vertical faults. Each individual region is assumed to be homogeneous and isotropic with uniform thickness,

**Fig. 1** Schematic of the two-dimensional top view of the multi-region linear composite model for a multistage-fractured horizontal well with secondary fractures



while the physical properties of each region differ from the others. The faults are assumed to be partially communicating with a fault skin. The external boundaries at the top and bottom are closed. A multistage-fractured horizontal well with arbitrarily distributed secondary fractures is positioned in all regions. The primary fractures (PFs) and secondary fractures (SFs) are assumed to have a rectangular shape with constant fracture length, width, and permeability. The system can be treated as a two-dimensional system since both types of fractures are assumed to be fully penetrating.

Other assumptions of the conceptual model include the following:

1. Fluids are in single-phase, slightly compressible, with a constant compressibility.
2. Isothermal Darcy's law is followed.
3. The effects of the gravity and capillary pressure are ignored.
4. The initial formation pressure throughout the reservoir is equal to  $p_i$ .
5. A constant production rate is expected at the MFHWs.

## Mathematical model

### The multi-region composite matrix systems

The governing differential equations for the two-dimensional pressure distribution in the composite systems with partially-communicating faults are written as

$$\left(\frac{k}{\mu}\right)_j \frac{\partial^2 p_j}{\partial x^2} + \left(\frac{k}{\mu}\right)_j \frac{\partial^2 p_j}{\partial y^2} = (\phi C_t)_j \frac{\partial p_j}{\partial t} \tag{1}$$

The initial condition is expressed as

$$p_j|_{t=0} = p_i \tag{2}$$

The connecting conditions between regions with the partially-communicating faults (Abbaszadeh and Cinco-Ley 1995; Rahman et al. 2003; Deng et al. 2022) are

$$\left(\frac{kh}{\mu}\right)_j \frac{\partial p_j}{\partial x} \Big|_{x=x_j} = \left(\frac{kh}{\mu}\right)_{j+1} \frac{\partial p_{j+1}}{\partial x} \Big|_{x=x_j} \tag{3}$$

$$(p_{j+1} - p_j)_{x=x_j} = \left[ \frac{2\mu w_a}{k_a h} \right]_j \left(\frac{kh}{\mu}\right)_j \frac{\partial p_j}{\partial x} \Big|_{x=x_j} \tag{4}$$

The external boundary conditions in  $x$  and  $y$  direction are

$$\frac{\partial p_1}{\partial x} \Big|_{x=0} = \frac{\partial p_N}{\partial x} \Big|_{x=x_N} = 0 \tag{5}$$

$$\frac{\partial p_j}{\partial x} \Big|_{y=0} = \frac{\partial p_j}{\partial x} \Big|_{y=y_e} = 0 \tag{6}$$

Note:  $x_N=x_e$  where  $p$  is the pressure, MPa;  $p_i$  is the initial reservoir pressure, MPa;  $\mu$  is fluid viscosity, mPa-s;  $k$  is the reservoir permeability, mD;  $\phi$  is the rock porosity, %;  $C_t$  is the total compressibility, MPa<sup>-1</sup>;  $h$  is the reservoir thickness, m;  $x$  and  $y$  are the Cartesian coordinates, m;  $x_j$  is the distance from the fault  $j$  to the original point of the coordinate;  $x_e$  is the length of the reservoir, m;  $y_e$  is the width of the reservoir, m;  $k_a$  and  $w_a$  are the permeability and half-width of a fault, respectively. The subscript  $j$  represents the region number,  $j = 1, \dots, N$ .

Using the dimensionless variables defined in Table 1, the aforementioned transient flow equations (i.e., Eqs. 1–6) for the matrix flow can be rewritten in a dimensionless form as:

$$\frac{\partial^2 p_{jD}}{\partial x_D^2} + \frac{\partial^2 p_{jD}}{\partial y_D^2} = \eta_{\min,j} \frac{\partial p_{jD}}{\partial t_D} \tag{7}$$

$$p_{jD}|_{t_D=0} = 0 \tag{8}$$

$$\frac{\partial p_{jD}}{\partial x_D} \Big|_{x_D=x_{jD}} = \lambda_{j+1,j} \frac{\partial p_{j+1D}}{\partial x_D} \Big|_{x_D=x_{jD}} \tag{9}$$

$$(p_{j+1D} - p_{jD})_{x_D=x_{jD}} = S_{aj} \frac{\partial p_{jD}}{\partial x_D} \Big|_{x=x_{jD}} \tag{10}$$

$$\frac{\partial p_{1D}}{\partial x_D} \Big|_{x=0} = \frac{\partial p_{ND}}{\partial x_D} \Big|_{x_D=x_{ND}} = 0 \tag{11}$$

$$\frac{\partial p_{jD}}{\partial x_D} \Big|_{y_D=0} = \frac{\partial p_{jD}}{\partial x_D} \Big|_{y_D=y_{eD}} = 0 \tag{12}$$

### Fractures systems

In view of the asymmetrical distribution of fractures system, the left wing and right wing of one primary fracture are regarded as individual primary fracture, respectively. Hence, there are  $2N_{PF}$  primary fracture parts considered in the model.

The governing differential equations for one-dimensional pressure distribution in  $l$ -th fracture are given by (Cinco-Ley and Meng 1988; Chen et al. 2016a)

**Table 1** Definitions of the dimensionless variables

Dimensionless pressure	$p_D = \frac{2\pi\lambda_{\min}h}{q_B}(p - p_i)$ , where $\lambda_{\min} = \left(\frac{k}{\mu}\right)_{\min}$
Dimensionless time	$t_D = \frac{\eta_{\min}}{h^2}t$ , where $\eta_{\min} = \left(\frac{k}{\phi\mu C_v}\right)_{\min}$
Dimensionless distance	$x_D = \frac{x}{h}$ , $x_{fD} = \frac{x_f}{h}$ , $x_{eD} = \frac{x_e}{h}$ , $y_D = \frac{y}{h}$ , $y_{eD} = \frac{y_e}{h}$ ,
Mobility ratio	$\lambda_{j+1,j} = \lambda_{j+1}/\lambda_j$ , where $\lambda_j = \frac{k_j}{\mu_j}$
Storativity ratio	$\omega_{\min,j} = \omega_{\min}/\omega_j$ , where $\omega_j = (\phi C_v)_j$
Fault skin	$S_{aj} = \frac{\lambda_j}{h(\lambda_a/2w_a)_j}$
Dimensionless fracture conductivity	$F_{fCD} = \frac{k_f w_f}{k_{\min} h}$
Diffusivity ratio	$\eta_{\min,j} = \left(\frac{k}{\phi C_v \mu}\right)_{\min} / \left(\frac{k}{\phi C_v \mu}\right)_j = \lambda_{\min,j} / \omega_{\min,j}$
Dimensionless flow rate	$q_{fLD} = \frac{2q_{fl}x_{fl}h}{q_B}$ , $q_{w/LD} = \frac{q_{wfl}}{q_B}$
Dimensionless wellbore storage coefficient	$C_D = \frac{C}{2\pi h(\phi C_v)_{\min} h^2}$

$$\left(\frac{k}{\mu}\right)_f \frac{\partial^2 p_{fl}}{\partial \hat{x}_{fl}^2} + \frac{q_{fl}}{hw_{fl}} = 0 \tag{13}$$

The initial condition is

$$p_{fl} \Big|_{t=0} = p_i \tag{14}$$

The inner boundary condition is

$$\left(\frac{k}{\mu}\right)_f w_{fl} h \frac{\partial p_{fl}}{\partial \hat{x}_{fl}} \Big|_{\hat{x}_{fl}=0} = q_{wfl} \tag{15}$$

The external boundary condition is

$$\frac{\partial p_{fl}}{\partial \hat{x}_{fl}} \Big|_{\hat{x}_{fl}=L_{fl}} = 0 \tag{16}$$

where subscript *f* can represent primary fracture (PF) or secondary fracture (SF); subscript *l* represents the fracture number,  $l = 1, \dots, N_{PF}$  for PF and  $l = 1, \dots, N_{SF}$  for SF;  $\hat{x}_{fl}$  is the local Cartesian coordinate system associated with the *l*-th fracture;  $w_{fl}$  is the width of the *l*-th fracture;

$L_{PF_l}$  is the fracture length for the *l*-th primary fracture part (it is equal to the primary fracture half-length if the primary fracture is symmetric about the horizontal well);  $L_{SF_l}$  is the fracture length for the *l*-th secondary fracture;  $q_{fl}$  is the flow rate of the *l*-th fracture face;  $q_{wPF_l}$  is the flow rate from the *l*-th primary fracture to wellbore; and  $q_{wSF_l}$  is the flow rate from the *l*-th secondary fracture to the primary fracture connected it.

The transient flow equations (Eqs. 13–16) for the fractures flow can be given by following dimensionless form using dimensionless variables defined in Table 1:

$$\frac{\partial^2 p_{fD}}{\partial \hat{x}_{fD}^2} - \frac{2\pi}{F_{fCD}} q_{fD} = 0 \tag{17}$$

$$p_{fD}(t_D = 0) = 0 \tag{18}$$

$$\frac{\partial p_{fD}}{\partial \hat{x}_{fD}} \Big|_{\hat{x}_{fD}=0} = \frac{2\pi}{F_{fCD}} q_{wflD} \tag{19}$$

$$\frac{\partial p_{fD}}{\partial \hat{x}_{fD}} \Big|_{\hat{x}_{fD}=L_{fD}} = 0 \tag{20}$$

### Model solutions

Firstly, each primary fracture and secondary fracture is divided into  $M_{PF}$  and  $M_{SF}$  discrete segments respectively to obtain the solution for this system consisting of  $N_{PF}$  primary fractures ( $2N_{PF}$  primary fractures part) and  $N_{SF}$  secondary fractures, as shown in Fig. 2. The flow rate is assumed to be uniform in each discrete segment. The pressure responses caused by these fracture segments are calculated.

### Solution for Fluid flow in multi-region composite matrix systems

Taking the Laplace transformation with respect to  $t_D$  in Eqs. 7–12 yields,

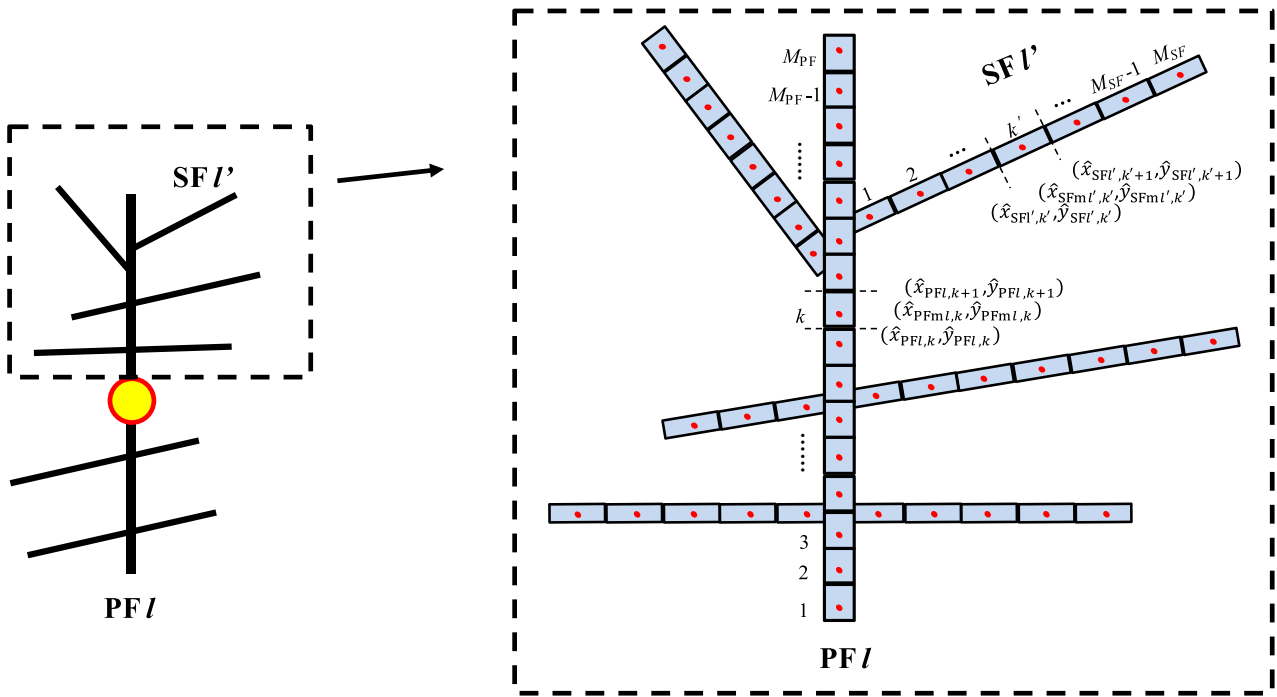


Fig. 2 Schematic of the discretization of a primary fracture with secondary fractures

$$\frac{\partial^2 \bar{p}_{jD}}{\partial x_D^2} + \frac{\partial^2 \bar{p}_{jD}}{\partial y_D^2} = \eta_{\min,j} u_j \bar{p}_{jD} \tag{21}$$

$$\left. \frac{\partial \bar{p}_{jD}}{\partial y_D} \right|_{y_D=0} = \left. \frac{\partial \bar{p}_{jD}}{\partial y_D} \right|_{y_D=y_{eD}} = 0 \tag{25}$$

$$\left. \frac{\partial \bar{p}_{jD}}{\partial x_D} \right|_{x_D=x_{jD}} = \lambda_{j+1,j} \left. \frac{\partial \bar{p}_{j+1D}}{\partial x_D} \right|_{x_D=x_{jD}} \tag{22}$$

In Eq. 21,  $u_j = sf_j(s)$  is a parameter to extend the solution into dual-porosity idealization of naturally fractured reservoirs (Ozkan and Raghavan 1991a, 1991b).  $s$  is the Laplace transform variable based on  $t_D$  and  $f_j(s)$  is given by

$$f_j(s) = \begin{cases} 1 & \text{for homogeneous reservoir} \\ \frac{\omega_{NFj}s(1-\omega_{NFj}) + \chi_{mNFj}}{s(1-\omega_{NFj}) + \chi_{mNFj}} & \text{for pseudosteady dual - porosity reservoir} \end{cases} \tag{26}$$

$$(\bar{p}_{j+1D} - \bar{p}_{jD}) \Big|_{x_D=x_{jD}} = S_{aj} \left. \frac{\partial \bar{p}_{jD}}{\partial x_D} \right|_{x_D=x_{jD}} \tag{23}$$

where  $\chi_{mNFj}$  is the inter-porosity flow coefficient in region  $j$ ,  $\omega_{NFj}$  is the storage ratio between naturally fractures and matrix in region  $j$ .

$$\left. \frac{\partial \bar{p}_{1D}}{\partial x_D} \right|_{x_D=0} = \left. \frac{\partial \bar{p}_{ND}}{\partial x_D} \right|_{x_D=x_{ND}} = 0 \tag{24}$$

We first consider the pressure response caused by a fracture segment in the multi-region composite matrix system. Using the Green’s function method (Raghavan 2010; Deng et al. 2017, 2022), the Laplace domain solution for a fracture segment in the multi-region composite matrix system,  $\bar{p}_{fsj,l,kD}$ , can be expressed as:

$$\bar{p}_{fsj,l,kD} = \bar{p}_{hfj,l,kD} + \bar{p}_{nsfj,l,kD} \text{ for the source region, where segment located} \tag{27}$$



$$\bar{p}_{fsj,l,kD} = \bar{p}_{nsfj,l,kD} \text{ for the no - source region} \tag{28}$$

where  $\bar{p}_{hfj,l,kD}$  is the solution for the  $k$ -th segment of the  $l$ -th fracture in a homogeneous rectangular banded system with the properties of the  $j$ -th region and  $\bar{p}_{nsfj,l,kD}$ , which satisfies the Eq. 21, is the no-source solution to a rectangular banded linear composite system for the  $j$ -th region.

Considering the azimuth of fracture segment,  $\bar{p}_{hfj,l,kD}$  is given by:

$$\bar{p}_{hfj,l,kD}(x_D, y_D) = \frac{\pi \bar{q}_{l,kD}}{2y_{eD} \lambda_{j,\min}} \int_{x_{fl,kD}}^{x_{fl,k+1D}} \left[ \frac{G(x_D, y_D, x'_D, \tan(\theta_{fl})(x'_D - x_{wflD}) + y_{wflD})}{\sqrt{1 + (\tan \theta_{fl})^2}} \right] dx'_D \tag{29}$$

$$G(x_D, y_D, x'_D, y'_D) = \sum_{m=0}^{\infty} \epsilon_m \cos\left(\frac{m\pi y_D}{y_{eD}}\right) \cos\left(\frac{m\pi y'_D}{y_{eD}}\right) \frac{\cosh(\gamma_{m,j} \tilde{x}_{D1}) + \cosh(\gamma_{m,j} \tilde{x}_{D2})}{\gamma_{m,j} \times \sinh(\gamma_{m,j} x_{eD})} \tag{30}$$

where  $\bar{q}_{l,kD}$  is the dimensionless flow rate from matrix from a fracture segment in Laplace domain,  $x_{fl,kD}$  and  $x_{fl,k+1D}$  are the value of starting and ending  $x$  coordinates of the  $k$ -th segment of the  $l$ -th fracture, respectively,  $\theta_{fl}$  is the azimuth between the  $l$ -th fracture segment and  $x$  axis,  $x_{wflD}$  and  $y_{wflD}$  are the value of starting coordinates of the starting  $l$ -th

$$\bar{p}_{nsfj,l,kD} = \frac{1}{2} \frac{\pi}{y_{eD}} \bar{q}_{l,kD} \sum_{m=0}^{\infty} \left\{ \begin{aligned} &\epsilon_m \cos\left(\frac{m\pi y_D}{y_{eD}}\right) \\ &\times \left( c_{m,j,l,k} e^{\gamma_{m,j}(x_D - x_{jD})} + d_{m,j,l,k} e^{\gamma_{m,j}(x_{j-1D} - x_D)} \right) \end{aligned} \right\} \tag{31}$$

where  $c_{m,j,l,k}$  and  $d_{m,j,l,k}$  are coefficient matrix.

Utilizing the superposition principle to all fracture segments in all regions, the dimensionless Laplace domain solution in the multi-region composite matrix system can

be written as

$$\bar{p}_{jD} = \sum_{l=1}^{2N_{PF}} \sum_{k=1}^{M_{PF}} \bar{p}_{PFsj,l,kD} + \sum_{l'=1}^{N_{SF}} \sum_{k'=1}^{M_{SF}} \bar{p}_{SFsj,l,kD} \tag{32}$$

According to Eqs. 29–30, Eq. 32 can be rewritten as

$$\bar{p}_{jD} = \sum_{l=1}^{2N_{PF}} \sum_{k=1}^{M_{PF}} \bar{q}_{l,kD} S_{fsj,l,kD} + \sum_{l'=1}^{N_{SF}} \sum_{k'=1}^{M_{SF}} \bar{q}_{l',k'D} S_{fsj,l',k'D} \tag{33}$$

where

$$S_{fsj,l,kD} = \frac{\pi}{2y_{eD}} \left\{ \begin{aligned} &\int_{x_{fl,kD}}^{x_{fl,k+1D}} \left[ \frac{G(x_D, y_D, x'_D, \tan(\theta_{fl})(x'_D - x_{wflD}) + y_{wflD})}{\sqrt{1 + (\tan \theta_{fl})^2}} \right] dx'_D \\ &+ \sum_{m=0}^{\infty} \left\{ \begin{aligned} &\epsilon_m \cos\left(\frac{m\pi y_D}{y_{eD}}\right) \\ &\times \left( c_{m,j,l,k} e^{\gamma_{m,j}(x_D - x_{jD})} + d_{m,j,l,k} e^{\gamma_{m,j}(x_{j-1D} - x_D)} \right) \end{aligned} \right\} \end{aligned} \right\} \tag{34}$$

fracture,  $\tilde{x}_{D1} = x_{eD} - |x_D - x'_D|$ ,  $\tilde{x}_{D2} = x_{eD} - |x_D + x'_D|$

$$\gamma_{m,j} = \sqrt{(m\pi/y_{eD})^2 + \eta_{\min,j} u} \text{ and } \epsilon_m = \begin{cases} 1 & m = 0 \\ 2 & m \geq 1 \end{cases}$$

Next, by applying the method of finite Fourier cosine transform and its inverse transform to Eqs. 21–25, the no-source solution to a rectangular banded linear composite system for the  $j$ -th region,  $\bar{p}_{nsfj,l,kD}$ , can be obtained. The detailed derivation of the Laplace domain solution is provided in Appendix A, and the resulting expression is as follows:

Hence, the dimensionless pressure on the  $k$ -th segment of  $l$ -th fracture can be rewritten as

$$\bar{p}_{fj,l,kD} = \sum_{l=1}^{2N_{PF}} \sum_{k=1}^{M_{PF}} \bar{q}_{PF,l,kD} S_{PFsj,l,kD} + \sum_{l'=1}^{N_{SF}} \sum_{k'=1}^{M_{SF}} \bar{q}_{SFl,k'D} S_{SFsj,l',k'D} \tag{35}$$



### Solution of fluid flow in the fracture system

The dimensionless pressure in the  $l$ -th primary fracture in the Laplace domain, according to Eqs. 17–20 is expressed as (Cinco-Ley et al. 1988)

$$\bar{p}_{wD} - \bar{p}_{PF/D} = \frac{\pi \hat{x}_{PF/D}}{F_{PFCDI}} \bar{q}_{wPF/D} - \frac{\pi}{F_{PFCDI}} \int_0^{\hat{x}_{PF/D}} \int_0^v \bar{q}_{PF/D} d\hat{x}_{PF/D} dv \tag{36}$$

The dimensionless pressure in the  $l$ -th secondary fracture in the Laplace domain, according to Eqs. 17–20 is expressed as (Chen et al. 2016a)

$$\bar{p}_{interSF/D} - \bar{p}_{SF/D} = \frac{\pi \hat{x}_{SF/D}}{F_{SFCDI}} \bar{q}_{wSF/D} - \frac{\pi}{F_{SFCDI}} \int_0^{\hat{x}_{SF/D}} \int_0^v \bar{q}_{SF/D} d\hat{x}_{SF/D} dv \tag{37}$$

where  $\bar{p}_{wD}$  is the dimensionless wellbore pressure in the Laplace domain,  $\bar{p}_{interSF/D}$  is the dimensionless pressure of intersectional segment in the  $l$ -th secondary fracture in the Laplace domain.

Equations 36 and 37 can be discretized respectively as follows:

For the primary fracture

$$\bar{p}_{wD} - \bar{p}_{PF/D}(\hat{x}_{PFm,l,kD}) = \left\{ \begin{array}{l} \frac{\pi \hat{x}_{PFm,l,kD}}{F_{PFCDI}} \sum_{i=1}^{M_{PF}} \bar{q}_{PF,iD} \\ - \frac{\pi}{F_{PFCDI}} \sum_{i=1}^{k-1} \left[ \bar{q}_{PF,iD} \left( \frac{1}{2} \Delta \hat{x}_{PF/D}^2 + \Delta \hat{x}_{PF/D} (\hat{x}_{PFm,l,kD} - i \Delta \hat{x}_{PF/D}) \right) \right] \\ + \bar{q}_{PF,iD} \frac{\Delta \hat{x}_{PF/D}^2}{8} \end{array} \right\} \tag{38}$$

For the secondary fracture

$$\bar{p}_{interSF/D} - \bar{p}_{SF/D}(\hat{x}_{SFm,l,kD}) = \left\{ \begin{array}{l} \frac{\pi \hat{x}_{SFm,l,kD}}{F_{SFCDI}} \sum_{i=1}^{M_{SF}} \bar{q}_{SF,iD} \\ - \frac{\pi}{F_{SFCDI}} \sum_{i=1}^{k-1} \left[ \bar{q}_{SF,iD} \left( \frac{1}{2} \Delta \hat{x}_{SF/D}^2 + \Delta \hat{x}_{SF/D} (\hat{x}_{SFm,l,kD} - i \Delta \hat{x}_{SF/D}) \right) \right] \\ + \bar{q}_{SF,iD} \frac{\Delta \hat{x}_{SF/D}^2}{8} \end{array} \right\} \tag{39}$$

where  $\hat{x}_{PFm,l,kD}$  and  $\hat{x}_{SFm,l,kD}$  is the dimensionless distance of the midpoint of the  $k$ -th segment in the  $l$ -th primary fracture

and the  $l$ -th secondary fracture respectively;  $\Delta \hat{x}_{PF/D}$  and  $\Delta \hat{x}_{SF/D}$  is the dimensionless length of each segment of the  $l$ -th primary fracture and the  $l$ -th secondary fracture respectively, and  $\Delta \hat{x}_{PF/D} = \frac{L_{PF/D}}{M_{PF}}$ ,  $\Delta \hat{x}_{SF/D} = \frac{L_{SF/D}}{M_{SF}}$ .

### Solution of transient pressure in the complex systems

Considering the continuity condition in the intersectional segments between primary fractures and secondary fractures, the pressure and flow rate should satisfy

$$\bar{p}_{interPF/D} = \bar{p}_{interSF/D} \tag{40}$$

$$\sum_{k=1}^{M_{SF}} \bar{q}_{SF,kD} + \bar{q}_{interPF/D} = \bar{q}_{interPF/D}^* \tag{41}$$

where  $\bar{p}_{interPF/D}$  is the dimensionless pressure of intersectional segment in primary fracture connected to the  $l$ -th secondary fracture in the Laplace domain;  $\bar{q}_{interPF/D}$  is the dimensionless flow rate caused by the intersectional segment in primary fracture connected to the  $l$ -th secondary fracture in the Laplace domain;  $\bar{q}_{interPF/D}^*$  is the total dimensionless flow rate of intersectional segment in primary fracture connected to the  $l$ -th secondary fracture in the Laplace domain.

The total flow rate is described as the summation of the flow rate from each primary fracture segment. Thus,

$$\sum_{l=1}^{N_{PF}} \sum_{k=1}^{2M_{PF}} \bar{q}_{PF,l,kD}^* \Delta \hat{x}_{PF/D} = \frac{1}{s} \tag{42}$$

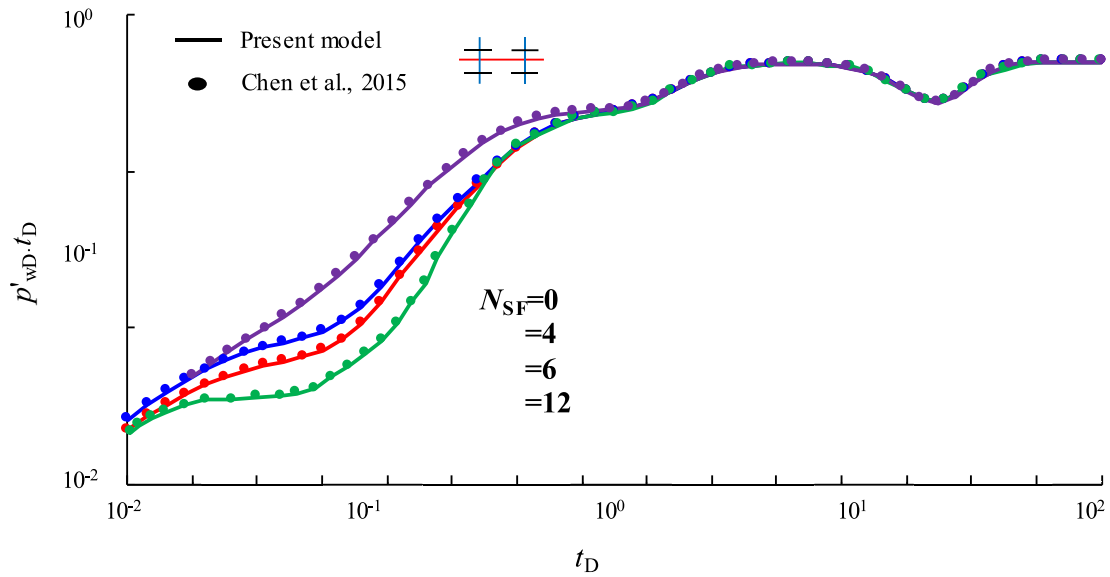


**Fig. 3** Performance comparison between the newly developed model and the homogeneous model (Chen et al. 2016a)

Substituting Eq. 41 into Eq. 42, and notice that  $\bar{q}_{PF,l,kD}^* = \bar{q}_{PF,l,kD}$  for all segments except intersectional segments we have

$$\sum_{l=1}^{N_{PF}} \sum_{k=1}^{M_{PF}} \bar{q}_{PF,l,kD} \Delta \hat{x}_{PF/D} + \sum_{l=1}^{N_{SF}} \sum_{k=1}^{M_{SF}} \bar{q}_{SF,l,kD} \Delta \hat{x}_{SF/D} = \frac{1}{s} \quad (43)$$

Then writing Eqs. 38 and 39 for each segment of each fracture and combining Eqs. 40 and 43 creates a system of  $2N_{PF} \times M_{PF} + N_{SF} \times M_{SF} + 1$  equations with  $2N_{PF} \times M_{PF} + N_{SF} \times M_{SF} + 1$  unknowns ( $\bar{q}_{PF,l,kD}, \bar{q}_{SF,l,kD}, \bar{p}_{wD}$ ). The unknown numbers can also be easily obtained using linear algebra.

Considering the effect of wellbore storage and the skin, the dimensionless wellbore pressure in Laplace domain can be obtained by the following:

$$\bar{p}_{wD} = \frac{s\bar{p}_{wD} + S}{s + C_D s^2 (s\bar{p}_{wD} + S)} \quad (44)$$

where  $C_D$  is the dimensionless wellbore storage coefficient, and  $S$  is the skin factor.

Noticed that we can also obtain the rate solution under constant pressure by using Duhamel principle (Everdingen and Hurst 1949), and its form is given as follows:

$$\bar{q}_{wD} = \frac{1}{s^2} \bar{p}_{wD} \quad (45)$$

**Fig. 4** Performance comparison between the newly developed model and the no- secondary fractures model (Wang et al. 2017)

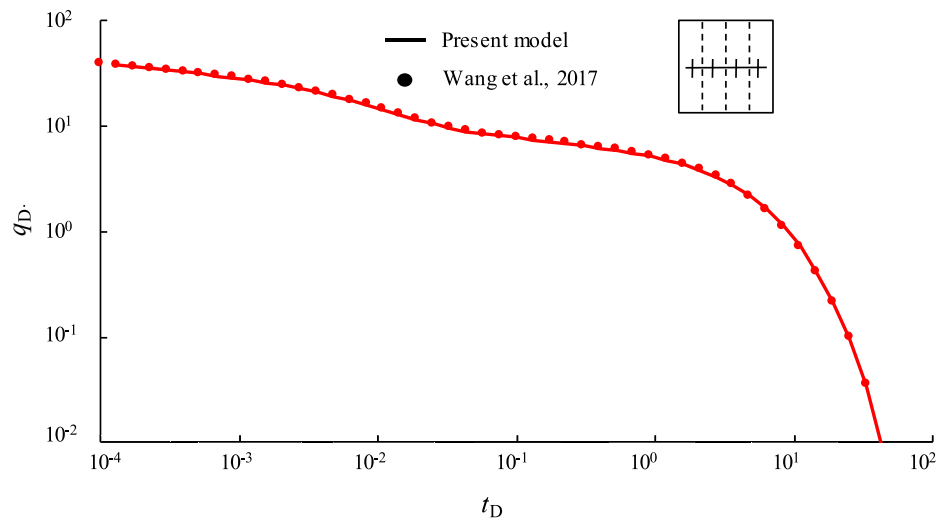


**Table 2** Default parameter values

$N_{PF}=2$	$N_{SF}=8$
$F_{PFCD}=200$	$F_{SFCD}=20$
$l_{PFD}=10$	$l_{SFD}=2$
$x_{wPF1D}=1875$	$\theta_{SPF}=90^\circ$
$y_{wPF1D}=2000$	$\Delta x_{wPF1D}=300$
$x_{eD}=4000$	$y_{eD}=4000$
$N=2$	$x_{1D}=2000$
$S_a=0$	$\lambda_{2,1}=2$
$\omega_{1,2}=1$	$S=0.01$
$C_D=1 \times 10^{-4}$	

The dimensionless wellbore pressure ( $p_{wD}$ ) can be obtained using the Stehfest numerical inversion to convert the Laplace domain solution  $\bar{p}_{wD}$  to  $p_{wD}$  (Stehfest 1970).

**Model validation**

The results of the newly developed model are compared with those from the two widely used models in the literature, one is the model of a MFHW with secondary fractures in an infinite homogeneous reservoir (Chen et al. 2016a) and the other is the model of MFHWs in a banded channel heterogeneous reservoir (Wang et al. 2017). Figure 3 illustrates the comparison between Chen et al.’s model and the newly developed model in the pressure derivative curve ( $p_{wD}'$  vs  $t_D$ ) under four sets of the number of secondary fractures ( $N_{SF}=0, 8, 12, 24$ ). It should be noted that, the four values of  $N_{SF}$  are set to 0, 4, 6, 12, respectively in, Chen et al.’s curves for consistency due to different definition of the number of secondary fractures between the two models. By setting an approximate infinite boundary (i.e.,  $x_{eD}=2 \times 10^6$ ,  $y_{eD}=2 \times 10^6$ ) and  $N=1$ (i.e., homogeneous reservoir), the newly developed model converges to a homogeneous model (Chen et al. 2016a). The other parameters used in Fig. 3

are as follow:  $N_{PF}=2$ ,  $\Delta x_{wPF1D}=250$  ( $\Delta x_{wPF1D}=x_{wPF2D}-x_{wPF1D}$ ),  $x_{PFD}=7.5$ ,  $l_{SFD}/x_{PFD}=2$ ,  $F_{PFCD}=80$ ,  $F_{SFCD}=20$ ,  $\chi_{mNF}=1 \times 10^{-8}$ ,  $\omega_{NF}=0.2$ .

Figure 4 shows the comparison between Wang et al.’s model and the newly developed model in the rate curve ( $q_{wD}$  vs  $t_D$ ) under a four-region heterogeneous case. By setting  $N_{SF}=0$  (no secondary fractures) and  $S_{aj}=0$  (no fault skin) the newly developed model converges to the no- secondary fractures model (Wang et al. 2017). The other parameters used in Fig. 4 are as follow:  $N_{PF}=4$ ,  $N=4$ ,  $x_{eD}=30$ ,  $y_{eD}=7$ ,  $\lambda_{2,1}=3$ ,  $\lambda_{3,2}=2$ ,  $\lambda_{4,3}=1.5$ ,  $\Delta x_{wPF1D}=6.67$ ,  $F_{PFCD}=35$ .

The good match between Figs. 3 and 4 shows that the newly developed model, in their simplified cases, converge to the existing models, and it also proves that the newly developed model is correct.

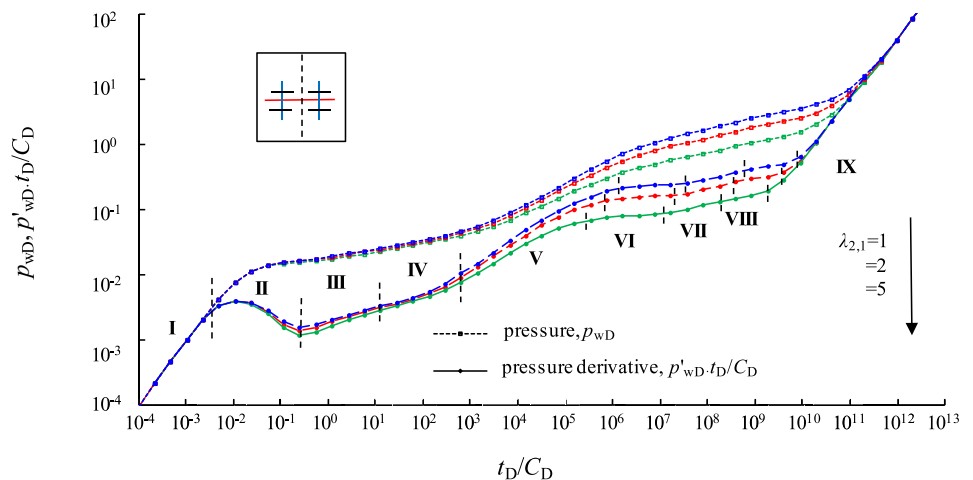
**Type curve construction and sensitivity analysis**

Solutions of the newly-developed models are calculated to obtain the standard log–log type curves, including the dimensionless pressure and its derivative with respect to the  $t_D/C_D$  of the transient pressure response. The main flow regimes are identified, and the effects of the relevant parameters on the pressure transient behavior are analyzed by analyzing the type curves. The default values of the parameters used in this section are shown in Table 2.

**Flow regimes recognition and effect of the characteristic parameters of reservoir heterogeneity**

Setting three values of  $\lambda_{2,1}$  (① $\lambda_{2,1}=1$ ; ② $\lambda_{2,1}=2$ ; ③ $\lambda_{2,1}=5$ ), with the other relevant parameters as presented in Table 2, three types of pressure transient behavior are obtained. Because the dimensionless pressure and time are based

**Fig. 5** Flow regimes of MFHWs with secondary fractures in heterogeneity reservoirs and effect of the permeability heterogeneity in type curves



on the parameter of the minimum conductivity region in our work, one can consider that the well is traversing many interfaces and draining higher permeability regions in the heterogeneous case.

Figure 5 shows the main flow regimes and the effect of permeability heterogeneity on the type curves related to pressure behavior characteristics of a MFHW with two primary fractures and four secondary fractures passing through two-region banded channel heterogeneous reservoir. It can be seen that there are nine main flow regimes in the type curves:

- I. *Wellbore storage regime* During this regime, the production is dominated by the fluids stored in the wellbore. The shape of the dimensionless wellbore pressure and its derivative curve is an upward straight line with a unit slope.
- II. *Skin effect regime* In this regime, the shape of the dimensionless wellbore derivative curve resembles a "hump".
- III. *Bilinear flow regime* During this regime, two linear flows occur simultaneously. One flows from the hydraulic fractures to the wellbore, while the other flows from the reservoir of region 1 to the hydraulic fracture. The derivative curve of bilinear flow regime is an upward straight line with a slope of 1/4.
- IV. *Fluid-feed regime* During this regime, fluid start to flow from the secondary fractures to the primary fractures. The derivative curve of the fluid-feed regime resembles a "dip".
- V. *First linear flow regime* The dimensionless wellbore pressure derivative curve is an upward straight line

with a slope of 0.5. The fluids mainly experience linear flow from the reservoir to the primary fractures during the first linear flow regime.

- VI. *Early pseudo-radial flow regime* During this regime, the slope of the dimensionless wellbore pressure derivative curves is zero, indicating a pseudo-radial flow from the reservoir to each of the primary fractures.
- VII. *Second linear flow regime* During this regime, the dimensionless wellbore pressure derivative curve is an upward straight line. This behavior is attributed to the interference of pressure waves from adjacent fractures during fracture production.
- VIII. *The second pseudo-radial flow regime* During this regime, the slope of the dimensionless wellbore pressure derivative curves is zero. This behavior indicates that the fluids experience radial flow from the reservoir to the MFHW, and this regime persists until the reservoir boundary is reached.
- IX. *Boundary-dominated flow regime* During this regime, the pressure front interacts with all closed boundaries. The curves of dimensionless wellbore pressure and its derivative follow unit-slope lines, indicating a pseudo-steady-state flow of fluids.

The contrast with the homogeneous case, as been seen from Fig. 5 reveals that permeability heterogeneity does not introduce a new, unique flow regime. However, it significantly influences the curves of all other flow regimes, except the wellbore storage and skin effect and boundary-dominated flow regimes. The vertical position of II–VIII flow regimes

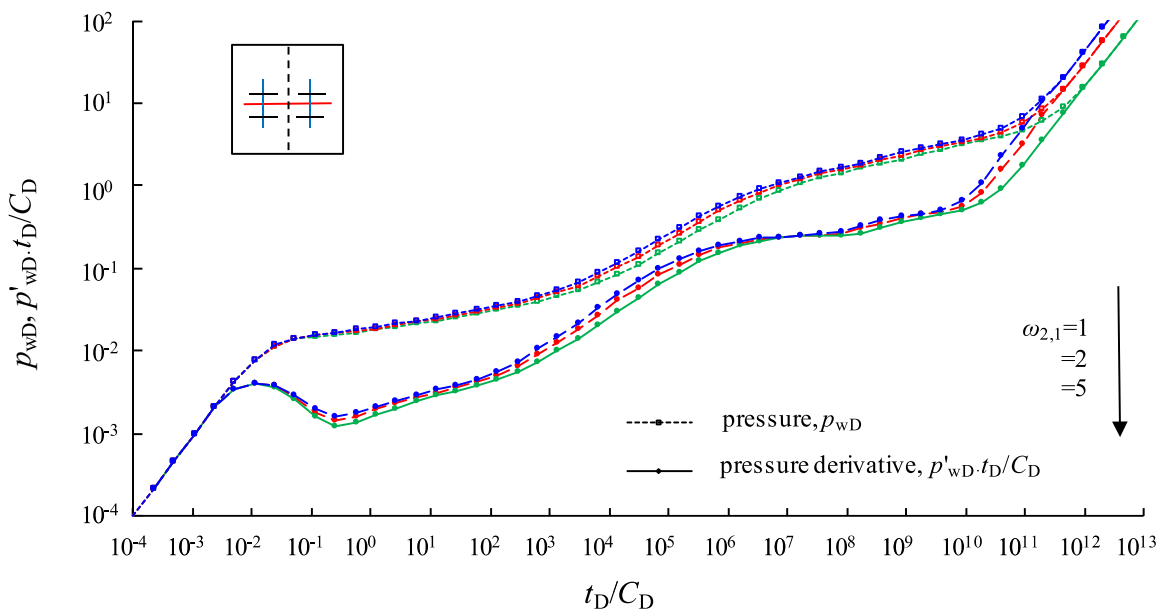
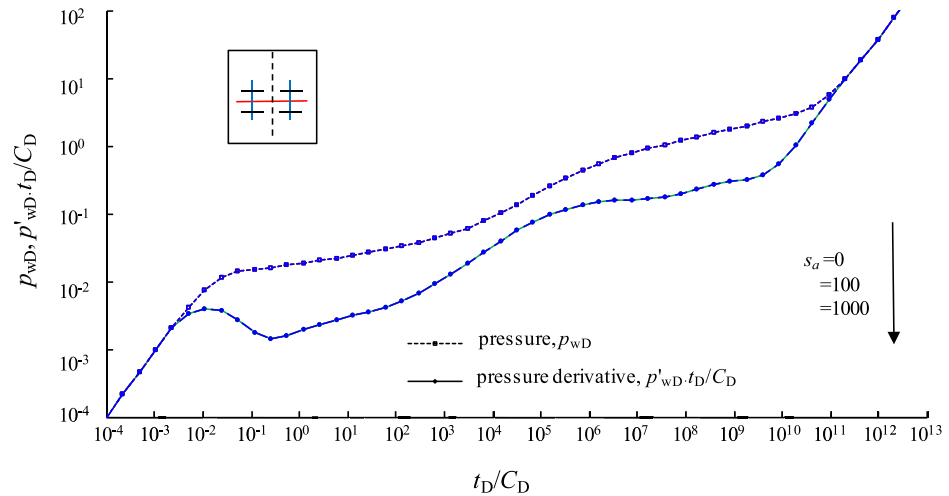
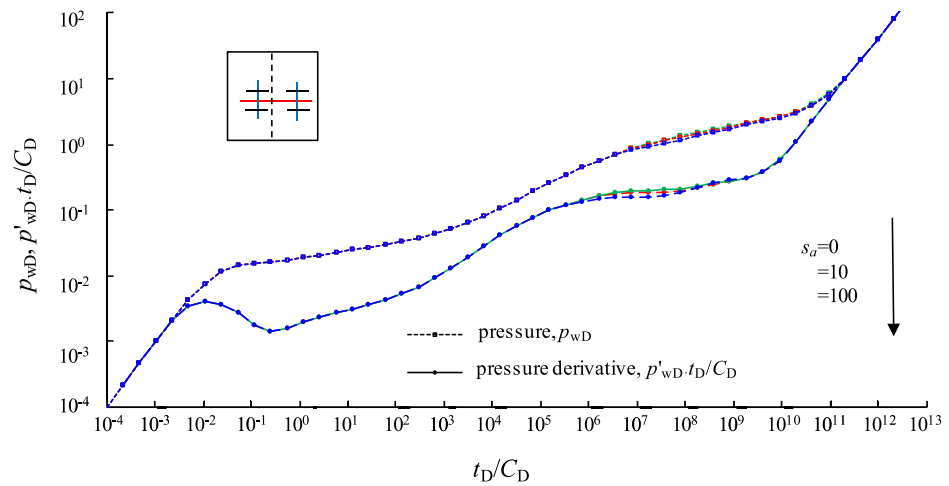


Fig. 6 Effect of the storativity ratio,  $\omega_{1,2}$

**Fig. 7** Effect of the fault skin,  $S_a$ , in the first scenario



**Fig. 8** Effect of the fault skin,  $S_a$ , in the second scenario



on curves gradually decreases in the heterogeneous case compared to that in the homogeneous case. A higher value of mobility ratio  $\lambda_{2,1}$  leads to a smaller pressure drop in the wellbore, and thus a greater difference from the homogeneous case. This is because the average permeability in the heterogeneous case is higher than that in the homogeneous case. Owing to the higher average permeability in the heterogeneous case, VI–VIII flow regimes appear earlier in the curves. This distinction is also notable when comparison to the pressure characteristics observed in heterogeneous cases where the well does not traverse distinct regions (Zhao et al. 2014; Deng et al. 2022). In such cases, permeability heterogeneity primarily influences the later radial/ pseudo-radial flow regime.

**Effect of the storativity heterogeneity**

The effect of storativity ratio,  $\omega_{2,1}$ , on the pressure transient behavior is illustrated in Fig. 6 It can be observed that  $\omega_{1,2}$  mainly influences the time of occurrence of all flow regimes

except the wellbore storage flow regime. A higher value of  $\omega_{2,1}$  results in a higher average storativity in the reservoir, consequently causing the II–IX flow regimes to appear later.

**Effect of the fault skin ( $S_a$ )**

Two scenarios of  $S_a$  are discussed: one is that the fault is located in the middle of two prime fractures ( $x_{wPFD1} = 1850$ ,  $x_{ID} = 2000$ ,  $x_{wPFD2} = 2150$ ) and the other is that the fault is located close to one of prime fractures ( $x_{wPFD1} = 1990$ ,  $x_{ID} = 2000$ ,  $x_{wPFD2} = 2290$ ). Three types of pressure transient behavior are obtained in two cases by setting three values of  $S_a$  (① $S_a = 0$ ; ② $S_a = 100$ ; ③ $S_a = 1000$ ). Figure 7 illustrates the impact of  $S_a$  on the pressure transient behavior in the first scenario. It is apparent that  $S_a$  exerts no discernible effect on the type curves in this instance. This lack of influence is attributed to the fault being positioned in the middle of each two primary fractures, where the pressure wave of two fractures interferes with each other. Essentially, the interference between the pressure waves in the middle of the two

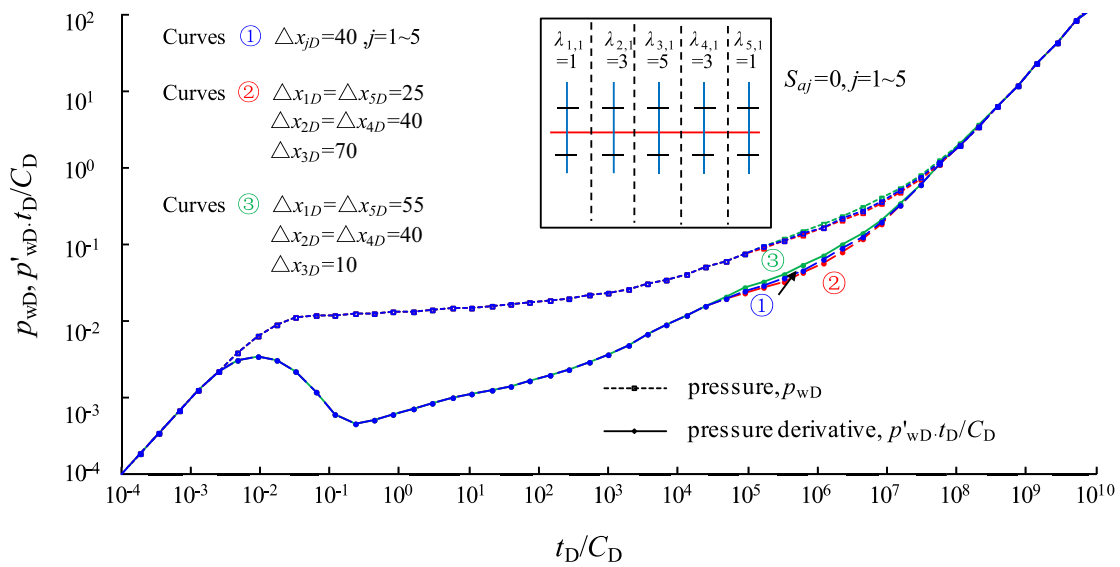


Fig. 9 Effect of the region area heterogeneity in no-fault skin case

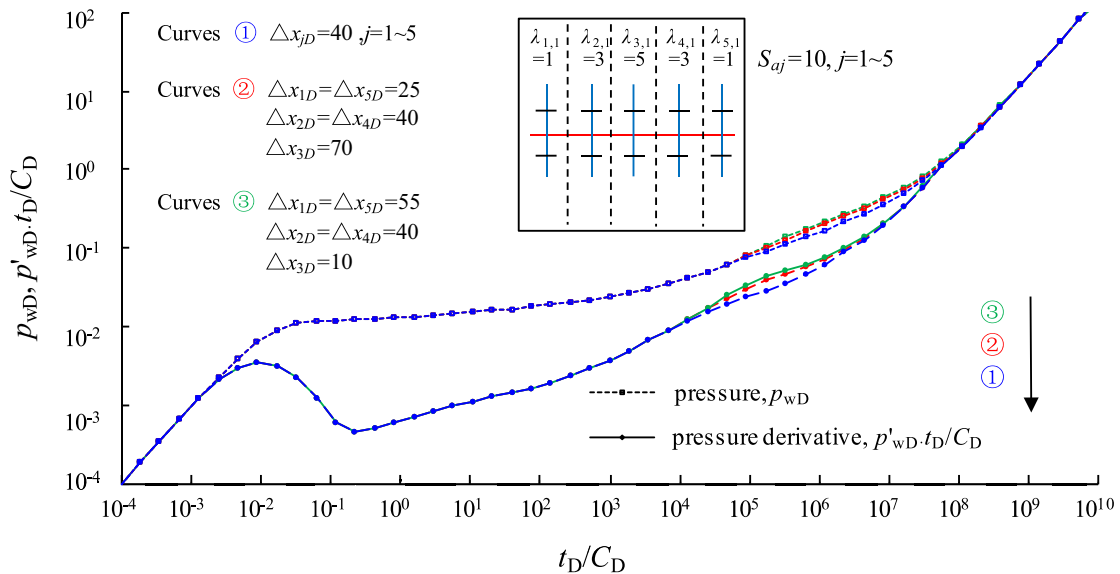


Fig. 10 Effect of the region area heterogeneity in fault skin case

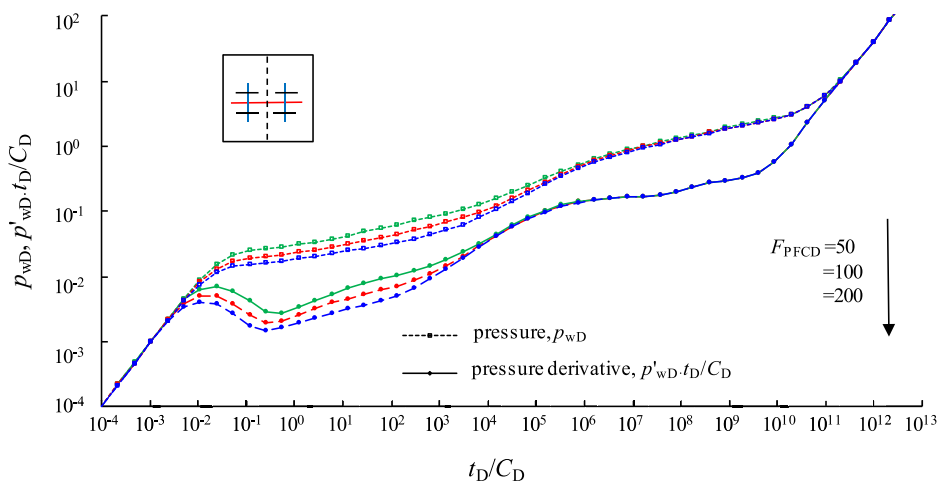
fractures creates an equivalent "sealed fault." Consequently, the influence of  $S_a$  is masked by the presence of this equivalent "sealed fault" on the curves in this particular case.

Figure 8 illustrates the effect of  $S_a$  on the pressure transient behavior in the second scenario. Notably,  $S_a$  influences both the early pseudo-radial flow regime and the second linear flow regime on the type curves. Due to the asymmetric position of fault, the effect of  $S_a$  is not masked by the influence of the equivalent "sealed fault". As  $S_a$  increases, a greater additional drawdown is required in the fault, resulting in an upward shift in the vertical position of the early pseudo-radial flow regime on the curves and a delayed appearance of the second linear flow regime.

### Effect of the region area heterogeneity

Figures 9 and 10 illustrate the effect of region area heterogeneity on the pressure transient behavior for a no-fault skin case ( $s_{aj}=0, j=1\sim 5$ ) and a fault skin case ( $s_{aj}=10, j=1\sim 5$ ) respectively. The horizontal well with five primary fractures and ten secondary fractures is positioned in a relatively small ( $x_{eD}=200, y_{eD}=200$ ) five-region composite reservoir. The mobility decreases with the increase in distance from the center ( $\lambda_{1,1}=1, \lambda_{2,1}=3, \lambda_{3,1}=5, \lambda_{4,1}=3, \lambda_{5,1}=1$ ), and a uniform distribution of fractures ( $\Delta x_{wPFD}=40$ ) is considered in the system. Similarly, three types of pressure transient behavior are observed in the small and large

**Fig. 11** Effect of the primary fracture conductivity,  $F_{PFCD}$



secondary fracture cases, by setting three sets of the length of region,  $\Delta x_{jD}$ , (①  $\Delta x_{jD} = 40, j = 1 \sim 5$ ; ②  $\Delta x_{1D} = \Delta x_{5D} = 25, \Delta x_{2D} = \Delta x_{4D} = 40, \Delta x_{3D} = 70$ ; ③  $\Delta x_{1D} = \Delta x_{5D} = 55, \Delta x_{2D} = \Delta x_{4D} = 40, \Delta x_{3D} = 10$ ).

It is evident that the early pseudo-radial flow regime and the second pseudo-radial flow regime are obscured by the second linear flow regime in the case of a relatively small reservoir and a small interval between fractures. This is because the impact of pressure interference between fractures and the effect of closed boundaries manifests early in this case. In addition, region area heterogeneity mainly influences the second linear flow regime in the type curves, as seen from Fig. 9. The I–V flow regime remain unchanged with variations in  $\Delta x_{jD}$  because the pressure response of three cases reflects the part of reservoir with same average permeability before the interference among fractures occurs. During the second linear flow regime, the pressure front reaches the entire reservoir. Therefore, the larger the region with higher permeability, the higher the average permeability of reservoir will be. Consequently, the lower the vertical position of second linear flow regime in the type curves appears.

**Fig. 12** Effect of the secondary fracture conductivity,  $F_{SFCD}$

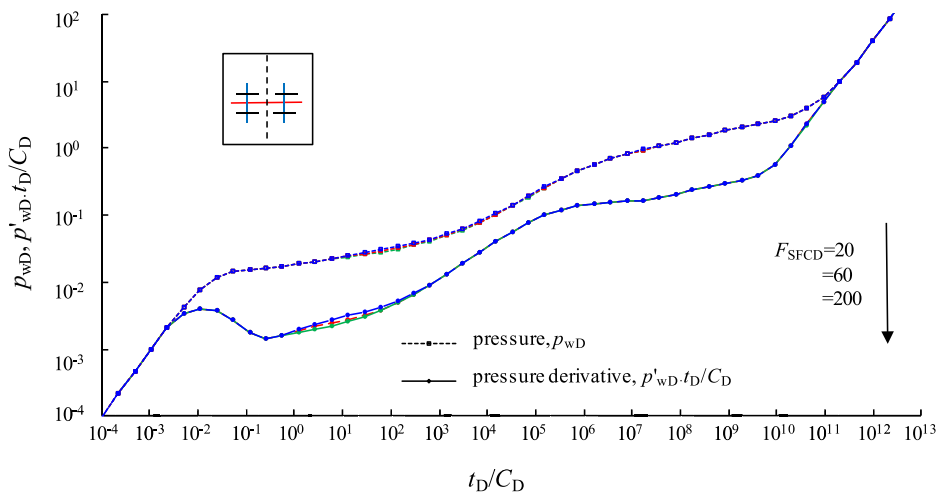


Figure 10 indicates that the impact of region area heterogeneity in the fault skin case differs from that in the no-fault skin case. Since the faults are asymmetrically positioned among the primary fractures (see Fig. 10, case ② and ③), the effect of fault skin is not obscured by the equivalent “sealed fault” effect in this case. Consequently, the vertical position of second linear flow regime increases in cases with region area heterogeneity (case ② and ③) in the curves. It is noteworthy that the pressure drop in the wellbore is smaller in case ② compared to case ③, attributed to the higher average permeability of the reservoir.

**Effect of the characteristic parameters of fractures system**

**Effect of the primary fracture-conductivity (FPFCD)**

Figure 11 illustrates the impact of  $F_{PFCD}$  on the pressure transient behavior. It is evident that  $F_{PFCD}$  influences the skin effect regime, bilinear flow regime, fluid-feed regime and first linear flow regime in the type curves. With an increase



**Fig. 13** Effect of the fracture-length ratio,  $l_{SF}/x_{PFD}$

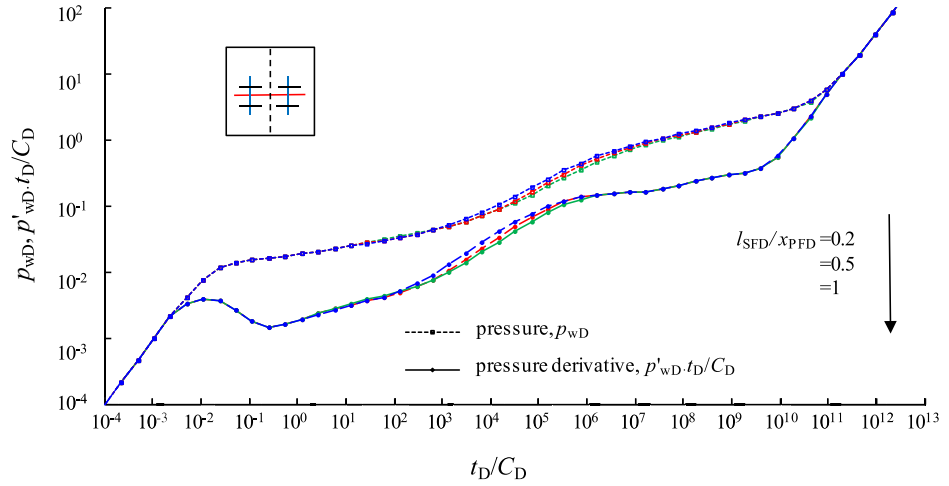


**Fig. 14** Effect of the secondary-fracture number,  $N_{SF}$

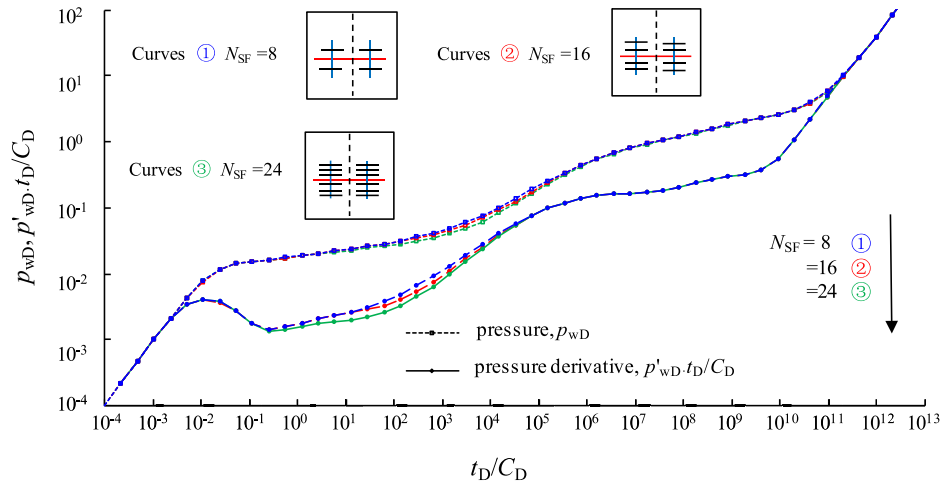
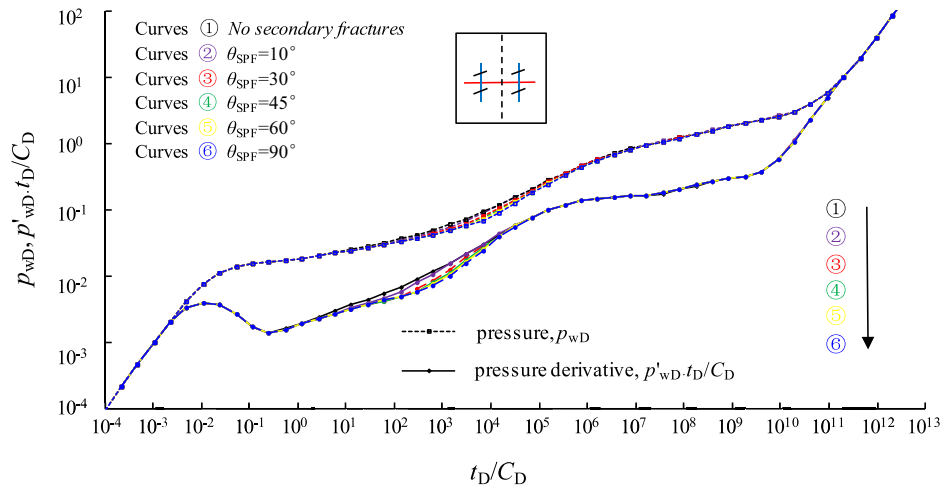


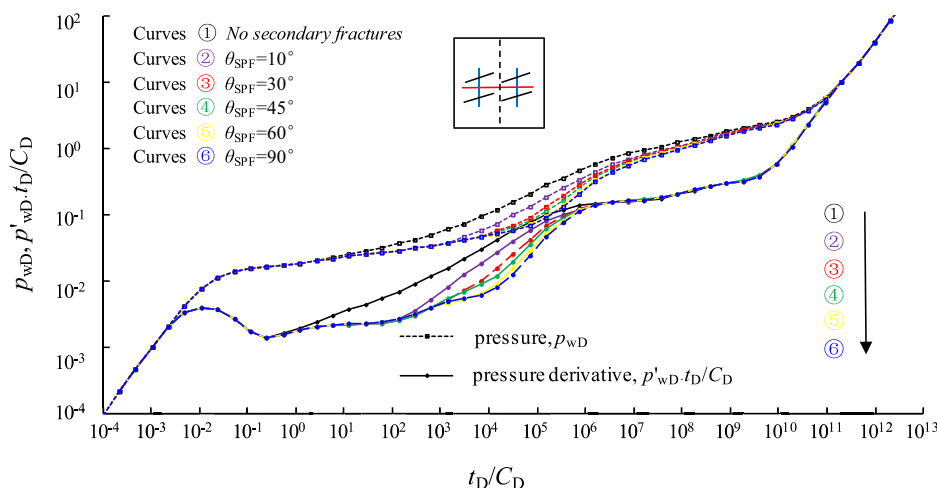
**Fig. 15** Effect of the azimuth angle between SF and PF,  $\theta_{SPF}$ , in small secondary fractures case



in the  $F_{PFC}$ , a smaller pressure drop is needed in the primary fractures. Consequently, the vertical position of the

II–V flow regimes decreases, and the duration of the bilinear flow regime and fluid-feed regime decreases.

**Fig. 16** Effect of the azimuth angle between SF and PF,  $\theta_{\text{SPF}}$ , in large secondary fractures case



### Effect of the secondary fracture-conductivity (FSFCD)

Figure 12 depicts the impact of  $F_{\text{SFCD}}$  on the pressure transient behavior. It is evident that  $F_{\text{SFCD}}$  influences the bilinear flow regime and fluid-feed regime in the type curves. With an increase in  $F_{\text{SFCD}}$ , a smaller pressure drop is required in the secondary fractures. Consequently, the duration of the bilinear flow regime decreases and the fluid-feed regime appears earlier.

### Effect of the fracture-length ratio (the ratio of the length of the primary fracture to the secondary fracture, $l_{\text{SFD}}/x_{\text{PFD}}$ )

Figure 13 illustrates the impact of  $l_{\text{SFD}}/x_{\text{PFD}}$  on the pressure transient behavior.  $l_{\text{SFD}}/x_{\text{PFD}}$  influences the fluid-feed regime and first linear flow regime in the type curves. As  $l_{\text{SFD}}/x_{\text{PFD}}$  increases, indicating relatively more reserves in the secondary fractures, the duration of the fluid-feed regime increases, and the vertical position of the first linear flow regime decreases.

### Effect of secondary-fracture number (NSF)

Figure 14 illustrates the impact of  $N_{\text{SF}}$  on the pressure transient behavior.  $N_{\text{SF}}$  influences the bilinear flow regime, fluid-feed regime and first linear flow regime in the type curves. An increase in the number of secondary fractures, for the same number of primary fractures, is equal to an increase in effective formation permeability around primary fractures. Consequently, in the case of a large  $N_{\text{SF}}$ , a smaller pressure drop is needed in the primary fractures. Thus, the vertical position of the fluid-feed regime decreases, the duration of the fluid-feed regime increases, and the duration of the bilinear flow regime decreases.

### Effect of azimuth angle between secondary-fracture and primary-fracture ( $\theta_{\text{SPF}}$ )

Figures 15 and 16 depict the effect of  $\theta_{\text{SPF}}$  on the pressure transient behavior for small secondary fractures case ( $l_{\text{SFD}}/x_{\text{PFD}}=0.2$ ;  $F_{\text{SFCD}}/F_{\text{PFCD}}=0.1$ ) and large secondary fractures case ( $l_{\text{SFD}}/x_{\text{PFD}}=1$ ;  $F_{\text{SFCD}}/F_{\text{PFCD}}=1$ ) respectively. Six types of pressure transient behavior are observed for a small secondary fractures case and a large secondary fractures case by setting five values of  $\theta_{\text{SPF}}$  (① $\theta_{\text{SPF}}=10$ ; ② $\theta_{\text{SPF}}=30$ ; ③ $\theta_{\text{SPF}}=45$ ; ④ $\theta_{\text{SPF}}=60$ ; ⑤ $\theta_{\text{SPF}}=90$ ) and a no-secondary fractures case ( $N_{\text{SF}}=0$ ).

It can be seen from Fig. 15 that  $\theta_{\text{SPF}}$  mainly influences the fluid-feed regime and first linear flow regime in the type curves. As the  $\theta_{\text{SPF}}$  approaches  $90^\circ$ , indicating a larger extent of the fractures system, a smaller pressure drop is required in the wellbore. Consequently, the vertical position of fluid-feed regime in type curves is decreases, and the appearance of the first linear flow regime is delayed.

Figure 16 illustrates the notable impact of  $\theta_{\text{SPF}}$  on the fluid-feed regime in the type curves for the large secondary fractures case. In this case, the first linear flow regime is gradually obscured as  $\theta_{\text{SPF}}$  approaches  $90^\circ$ , and the trend in the type curves resembles that observed in the case of small secondary fractures, albeit more pronounced.

## Conclusions

In this study, we developed a novel semi-analytical model to investigate the pressure transient behavior of multistage-fractured horizontal wells (MFHWs) with secondary fractures passing through banded channel heterogeneous reservoirs. The proposed approach integrates the source method and Green's function method, introducing an innovative technique for discretizing fractures without necessitating the discretization of interfaces. The model verification is performed through a comparative analysis with two established models from the existing

literature. Subsequently, we analyze the influences of reservoir heterogeneity, partially-communicating faults and fracture systems on transient behaviors. The following conclusions have been drawn from the study:

- (1) The pressure behavior of MFHWs passing through regions with different physical properties exhibits distinctive characteristics. In contrast to the homogeneous case, permeability heterogeneity does not introduce a new, unique flow regime. However, it significantly influences the curves of all other flow regimes, except the wellbore storage and skin effect and boundary-dominated flow regimes. This distinction is also notable in comparison to the pressure characteristics observed in heterogeneous cases where the well does not traverse distinct regions.
- (2) The fault skin influences the medium flow regimes when the fault is not positioned in the middle of each two primary fractures in the case of MFHWs passing through regions and faults. In the opposite case, the effect of the fault skin is masked by the equivalent “sealed fault” on the curves, and the pressure response characteristics of that case cannot reflect the connectivity of the fault.
- (3) Heterogeneity in region areas mainly influences the middle and late stages of flow regimes in the case of MFHWs passing through regions and faults, particularly when the connectivity of the fault is poor.
- (4) Fracture properties can influence the early flow regimes. A distinctive flow regime, identified by a ‘dip’ in derivative curves, emerges due to the secondary fractures connected to primary fractures, and this behavior strengthens and lengthens with higher fracture-length ratio, secondary fracture conductivity, and the number of secondary fractures.

### Appendix A

Applying the finite Fourier cosine transform with respect to  $y_D$  to Eqs. (21–25) and considering the case of a fracture segment, we obtain the following:

$$\frac{\partial^2 \tilde{p}_{fsj,l,kD}}{\partial x_D^2} - \gamma_{mj} \tilde{p}_{fsj,l,kD} = 0 \tag{A1}$$

$$\left. \frac{\partial \tilde{p}_{fsj,l,kD}}{\partial x_D} \right|_{x_D=x_{jD}} = \lambda_{j+1,j} \left. \frac{\partial \tilde{p}_{fsj+1,l,kD}}{\partial x_D} \right|_{x_D=x_{jD}} \tag{A2}$$

$$\left( \tilde{p}_{fsj+1,l,kD} - \tilde{p}_{fsj,l,kD} \right)_{x_D=x_{jD}} = S_{aj} \left. \frac{\partial \tilde{p}_{fsj,l,kD}}{\partial x_D} \right|_{x=x_{jD}} \tag{A3}$$

$$\left. \frac{\partial \tilde{p}_{fs1,l,kD}}{\partial x_D} \right|_{x_D=0} = \left. \frac{\partial \tilde{p}_{fsN,l,kD}}{\partial x_D} \right|_{x_D=x_{ND}} = 0 \tag{A4}$$

According to Eq. (27), the general form of the solution for Eq. (A1) can be given as.

For the source region,

$$\tilde{p}_{fsj,l,kD} = \tilde{p}_{hff,l,kD} + a_{m,j,l,k} e^{\gamma_{mj} x_D} + b_{m,j,l,k} e^{-\gamma_{mj} x_D} \tag{A5}$$

For the no-source region,

$$\tilde{p}_{fsj,l,kD} = a_{m,j,l,k} e^{\gamma_{mj} x_D} + b_{m,j,l,k} e^{-\gamma_{mj} x_D} \tag{A6}$$

where  $\tilde{p}_{hff,l,kD}$  can be obtained by using finite Fourier cosine transform to Eq. 29, and its form is as follow:

$$\tilde{p}_{hff,l,kD} = \bar{q}_{l,kD} O_{sj,l,k} \tag{A7}$$

$$O_{fsj,l,k} = \frac{\pi}{2} \int_{x_{\beta,kD}}^{x_{\beta,k+1D}} \left[ \frac{\cos \left( \frac{m\pi (\tan(\theta_{\beta}) (x'_D - x_{w\beta D}) + y_{w\beta D})}{y_{eD}} \right)}{\cosh(\gamma_m \hat{x}_{D1}) + \cosh(\gamma_m \hat{x}_{D2})} \times \frac{1}{\gamma_m \times \sinh(\gamma_m x_{eD})} \sqrt{1 + (\tan \theta_{\beta})^2} \right] dx'_D \tag{A8}$$

For ease of calculation, a transformation of the constants,  $a_{m_j,l,k}$  and  $b_{m_j,l,k}$ , are given as follows:

$$c_{m_j,l,k} = \frac{a_{m_j,l,k}}{\bar{q}_{l,kD} e^{-\gamma_{m_j} x_{jD}}} \quad (\text{A9})$$

$$d_{m_j,l,k} = \frac{b_{m_j,l,k}}{\bar{q}_{l,kD} e^{\gamma_{m_j} x_{j-1D}}} \quad (\text{A10})$$

Substituting Eqs. (A7–A10) into Eqs. (A5) and (A6), the general forms of the solution in Laplace- Fourier domain are obtained:

For the source region,

$$\bar{\bar{p}}_{f_{sj,l,kD}} = \bar{q}_{l,kD} \left[ O_{f_{sj,l,k}} + \left( c_{m_j,l,k} e^{\gamma_{m_j} (x_{jD} - x_{jD})} + d_{m_j,l,k} e^{\gamma_{m_j} (x_{j-1D} - x_{jD})} \right) \right] \quad (\text{A11})$$

For the no-source region,

$$\bar{\bar{p}}_{f_{sj,l,kD}} = \bar{q}_{l,kD} \left( c_{m_j,l,k} e^{\gamma_{m_j} (x_{jD} - x_{jD})} + d_{m_j,l,k} e^{\gamma_{m_j} (x_{j-1D} - x_{jD})} \right) \quad (\text{A12})$$

All constants,  $c_{m_j,l,k}$  and  $d_{m_j,l,k}$ , can be obtained by substituting Eqs. (A11) and (A12) into the interface connecting conditions of each region (Eqs. (A2) and (A3)) and boundary condition (Eq. (A4)).

Then we apply the finite Fourier inverse transform to Eq. (A11) results in Eq. (31).

**Acknowledgements** The authors would like to thank the NSFC (National Natural Science Foundation of China) for supporting this research through a Joint Fund of petroleum and chemical industry under Grant No. U1762109. This study was financially supported by Sichuan Science and Technology Program (2023NSFSC0427). The authors would also like to thank the reviewers and editors, whose critical comments were very helpful in preparing this article.

**Funding** This study was funded by the Joint Fund of petroleum and chemical industry under Grant No. U1762109 from NSFC (National Natural Science Foundation of China) and by the Sichuan Science and Technology Program (2023NSFSC0427).

## Declarations

**Conflict of interest** The authors declare that they have no conflict of interest.

**Human participants** All procedures performed in studies involving human participants were in accordance with the ethical standards of the institutional and/or national research committee and with the 1964 Helsinki declaration and its later amendments or comparable ethical standards. This article does not contain any studies with animals performed by any of the authors.

**Informed consent** Informed consent was obtained from all individual participants included in the study.

**Open Access** This article is licensed under a Creative Commons Attribution 4.0 International License, which permits use, sharing, adaptation, distribution and reproduction in any medium or format, as long

as you give appropriate credit to the original author(s) and the source, provide a link to the Creative Commons licence, and indicate if changes were made. The images or other third party material in this article are included in the article's Creative Commons licence, unless indicated otherwise in a credit line to the material. If material is not included in the article's Creative Commons licence and your intended use is not permitted by statutory regulation or exceeds the permitted use, you will need to obtain permission directly from the copyright holder. To view a copy of this licence, visit <http://creativecommons.org/licenses/by/4.0/>.

## References

- Abbaszadeh M, Cinco-Ley H (1995) Pressure-transient behavior in a reservoir with a finite-conductivity fault. *SPE Form Eval* 10(1):26–32. <https://doi.org/10.2118/24704-PA>
- Al Rbeawi S, Tiab D (2012) Effect of penetrating ratio on pressure behavior of horizontal wells with multiple-inclined hydraulic fractures. In: *SPE western regional meeting* <https://doi.org/10.2118/153788-MS>
- Brown M, Ozkan E, Raghavan R et al (2011) Practical solutions for pressure-transient responses of fractured horizontal wells in unconventional shale reservoirs. *SPE Res Eval Eng* 14(06):663–676. <https://doi.org/10.2118/125043-PA>
- Chen Z, Yu W (2022) A discrete model for pressure transient analysis in discretely fractured reservoirs. *SPE J* 27(03):1708–1728. <https://doi.org/10.2118/209214-PA>
- Chen Z, Liao X, Zhao X (2016a) A semianalytical approach for obtaining type curves of multiple-fractured horizontal wells with secondary-fracture networks. *SPE J* 21(02):538–549. <https://doi.org/10.2118/178913-PA>
- Chen Z, Liao X, Zhao X et al (2016b) Influence of magnitude and permeability of fracture networks on behaviors of vertical shale gas wells by a free-simulator approach. *J Pet Sci Eng* 147:261–272. <https://doi.org/10.1016/j.petrol.2016.06.006>
- Chen Z, Liao X, Sephehnoori K et al (2018) A semianalytical model for pressure-transient analysis of fractured wells in unconventional plays with arbitrarily distributed fracture networks. *SPE J* 23(06):2041–2059. <https://doi.org/10.2118/187290-PA>
- Chen Z, Liao X, Yu W et al (2019) Pressure-transient behaviors of wells in fractured reservoirs with natural-and hydraulic-fracture networks. *SPE J* 24(01):375–394. <https://doi.org/10.2118/194013-PA>
- Cheng L, Jia P, Rui Z et al (2017) Transient responses of multifractured systems with discrete secondary fractures in unconventional reservoirs. *J Nat Gas Sci Eng* 41:49–62. <https://doi.org/10.1016/j.jngse.2017.02.039>
- Chu H, Ma T, Gao Y, et al (2022) A novel semi-analytical model for the multiwell horizontal pad with stimulated reservoir volume. In: *International petroleum technology conference* <https://doi.org/10.2523/IPTC-22193-MS>
- Cinco-Ley, H., Meng, H. Z (1988) Pressure transient analysis of wells with finite conductivity vertical fractures in double porosity reservoirs. In: *SPE annual technical conference and exhibition* <https://doi.org/10.2118/18172-MS>
- Cuba PH, Miskimins JL, Anderson DS et al (2013) Impacts of diverse fluvial depositional environments on hydraulic fracture growth in tight gas reservoirs. *SPE Prod Oper* 28(01):8–25. <https://doi.org/10.2118/140413-PA>
- Cui X, Huang X, Chen T, et al (2021) Faulted feature detection in a tight sand gas reservoir based on steerable pyramid voting. In: *SEG international exposition and annual meeting* <https://doi.org/10.1190/segam2021-3584019.1>

- Daneshy AA (2003) Off-balance growth: a new concept in hydraulic fracturing. *J Pet Technol* 55(04):78–85. <https://doi.org/10.2118/80992-JPT>
- Deng Q, Nie RS, Jia YL et al (2015) A new analytical model for non-uniformly distributed multi-fractured system in shale gas reservoirs. *J Nat Gas Sci Eng* 27:719–737. <https://doi.org/10.1016/j.jngse.2015.09.015>
- Deng Q, Nie RS, Jia YL et al (2017) Pressure transient behavior of a fractured well in multi-region composite reservoirs. *J Pet Sci Eng* 158:535–553. <https://doi.org/10.1016/j.petrol.2017.08.079>
- Deng Q, Nie RS, Wang S et al (2022) Pressure transient analysis of a fractured well in multi-region linear composite reservoirs. *J Pet Sci Eng* 208:109262. <https://doi.org/10.1016/j.petrol.2021.109262>
- Guo F, Chen R, Yan W et al (2023) A new seven-region flow model for deliverability evaluation of multiply-fractured horizontal wells in tight oil fractal reservoir. *FRAC-TALS (fractals)* 31(08):1–17. <https://doi.org/10.1142/S0218348X23401734>
- Guo G L, Evans R D, Chang M M (1994) Pressure-transient behavior for a horizontal well intersecting multiple random discrete fractures. In: SPE annual technical conference and exhibition <https://doi.org/10.2118/28390-MS>
- Heidari Sureshjani M, Clarkson CR (2015) An analytical model for analyzing and forecasting production from multifractured horizontal wells with complex branched-fracture geometry. *SPE Res Eval Eng* 18(03):356–374. <https://doi.org/10.2118/176025-PA>
- Horne R N, Temeng K O (1995) Relative productivities and pressure transient modeling of horizontal wells with multiple fractures. In: SPE middle east oil show <https://doi.org/10.2118/29891-MS>
- Hwang Y S, Lin J, Zhu D. et al (2013) Predicting fractured well performance in naturally fractured reservoirs. In: International petroleum technology conference <https://doi.org/10.2523/IPTC-17010-MS>.
- Jia YL, Wang BC, Nie RS et al (2014) New transient-flow modeling of a multistage-fractured horizontal well. *J Geophys Eng* 11(01):015013. <https://doi.org/10.1088/1742-2132/11/1/015013>
- Jia P, Cheng L, Huang S et al (2016) A semi-analytical model for the flow behavior of naturally fractured formations with multi-scale fracture networks. *J Hydrol* 537:208–220. <https://doi.org/10.1016/j.jhydrol.2016.03.022>
- Kuchuk FJ, Habashy T (1997) Pressure behavior of laterally composite reservoirs. *SPE Form Eval* 12(01):47–56. <https://doi.org/10.2118/24678-PA>
- Lin J, Zhu D (2012) Predicting well performance in complex fracture systems by slab source method. In: SPE hydraulic fracturing technology conference <https://doi.org/10.2118/151960-MS>.
- McDowell, B, Plink-Björklund P (2013) Reservoir geometries and Facies associations of fluvial tight-gas sands, Williams fork formation, Rifle Gap, Colorado. In: Unconventional resources technology conference <https://doi.org/10.1190/urtec2013-261>
- Medeiros F, Ozkan E, Kazemi H (2008) Productivity and drainage area of fractured horizontal wells in tight gas reservoirs. *SPE Res Eval Eng* 11(05):902–911. <https://doi.org/10.2118/108110-PA>
- Murillo G G, Salguero J (2016) Conventional fracturing vs. complex fracturing network in tight turbidite oil deposits in Mexico. In: SPE Argentina exploration and production of unconventional resources symposium <https://doi.org/10.2118/180999-MS>
- Ozkan E, Raghavan R (1991a) New solutions for well-test-analysis problems: part 1-analytical considerations. *SPE Form Eval* 6(03):359–368. <https://doi.org/10.2118/18615-PA>
- Ozkan E, Raghavan R (1991b) New solutions for well-test-analysis problems: part 2—computational considerations and applications. *SPE Form Eval* 6(03):369–378. <https://doi.org/10.2118/18616-PA>
- Raghavan R (2010) A composite system with a planar interface. *J Pet Sci Eng* 70(3–4):229–234. <https://doi.org/10.1016/j.petrol.2009.11.015>
- Raghavan R, Chen CC, Agarwal B (1997) An analysis of horizontal wells intercepted by multiple fractures. *SPE J* 2(03):235–245. <https://doi.org/10.2118/27652-PA>
- Rahman N M, Miller M D, Mattar L (2003) Analytical solution to the transient-flow problems for a well located near a finite-conductivity fault in composite reservoirs. In: SPE annual technical conference and exhibition <https://doi.org/10.2118/84295-MS>
- Ramirez K M, Cuba P H, Miskimins J L, et al (2012) Integrating geology, hydraulic fracturing modeling, and reservoir simulation in the evaluation of complex fluvial tight gas reservoirs. In: SPE/EAGE European unconventional resources conference & exhibition <https://doi.org/10.2118/151931-MS>
- Ren JJ, Guo P (2015) A novel semi-analytical model for finite-conductivity multiple fractured horizontal wells in shale gas reservoirs. *J Nat Gas Sci Eng* 24:36–51. <https://doi.org/10.1016/j.jngse.2015.03.015>
- Shi W, Jiang Z, Gao M et al (2023) Analytical model for transient pressure analysis in a horizontal well intercepting with multiple faults in karst carbonate reservoirs. *J Pet Sci Eng* 220:111183. <https://doi.org/10.1016/j.petrol.2022.111183>
- Stalgorova K, Mattar L (2013) Analytical model for unconventional multifractured composite systems. *SPE Res Eval Eng* 16(03):246–256. <https://doi.org/10.2118/162516-PA>
- Stehfest H (1970) Numerical inversion of Laplace transform-algorithm 368. *Commun ACM* 13(1):47–49. <https://doi.org/10.1145/361953.361969>
- Tao H, Zhang L, Liu Q et al (2018) An analytical flow model for heterogeneous multi-fractured systems in shale gas reservoirs. *Energies* 11(12):3422. <https://doi.org/10.3390/en11123422>
- van Dijk J, Ajayi A T, De Vincenzi L, et al (2020) Fault and fracture network analyses and modeling in a challenging complex geological environment-paleozoic tight reservoirs in Algeria. In: International petroleum technology conference <https://doi.org/10.2523/IPTC-19969-MS>
- van Everdingen AF, Hurst W (1949) The application of the Laplace transformation to flow problems in reservoirs. *J Pet Technol* 12(1):305–324. <https://doi.org/10.2118/949305-G>
- Wan J, Aziz K (1999) Multiple hydraulic fractures in horizontal wells. In: SPE western regional meeting <https://doi.org/10.2118/54627-MS>
- Wang HT (2014) Performance of multiple fractured horizontal wells in shale gas reservoirs with consideration of multiple mechanisms. *J Hydrol* 510:299–312. <https://doi.org/10.1016/j.jhydrol.2013.12.019>
- Wang J, Wang XD, Dong WX (2017) Rate decline curves analysis of multistage-fractured horizontal wells in heterogeneous reservoirs. *J Hydrol* 553:527–539. <https://doi.org/10.1016/j.jhydrol.2017.08.024>
- Wang J, Qiang X, Ren Z et al (2023) Analytical model for the pressure performance analysis of multi-fractured horizontal wells in volcanic reservoirs. *Energies* 16(2):879. <https://doi.org/10.3390/en16020879>
- Weng X, Kresse O, Chuprakov D et al (2014) Applying complex fracture model and integrated workflow in unconventional reservoirs. *J Pet Sci Eng* 124:468–483. <https://doi.org/10.1016/j.petrol.2015.04.041>
- Wu J, Zhang J, Chang C et al (2020) A model for a multistage fractured horizontal well with rectangular SRV in a shale gas reservoir. *Geofluids* 2020:1–18. <https://doi.org/10.1155/2020/8845250>
- Xiao Y, Lu L, Zhang J, et al (2023) Slurry acid fracturing was first ever proposed to unlock the production potential in low permeability carbonate reservoir in central Iraq. In: SPE international hydraulic fracturing technology conference and exhibition <https://doi.org/10.2118/215708-MS>
- Xu Y, Li X, Liu Q (2020) Pressure performance of multi-stage fractured horizontal well with stimulated reservoir volume and

- irregular fractures distribution in shale gas reservoirs. *J Nat Gas Sci Eng* 77:103209. <https://doi.org/10.1016/j.jngse.2020.103209>
- Yao S, Zeng F, Liu H et al (2013) A semi-analytical model for multi-stage fractured horizontal wells. *J Hydrol* 507:201–212. <https://doi.org/10.1016/j.jhydrol.2013.10.033>
- Zeng J, Wang X, Guo J et al (2017) Composite linear flow model for multi-fractured horizontal wells in heterogeneous shale reservoir. *J Nat Gas Sci Eng* 38:527–548. <https://doi.org/10.1016/j.jngse.2017.01.005>
- Zeng J, Wang X, Guo J et al (2018) Composite linear flow model for multi-fractured horizontal wells in tight sand reservoirs with threshold pressure gradient. *J Petrol Sci Eng* 165:890–912. <https://doi.org/10.1016/j.petrol.2017.12.095>
- Zeng J, Wang X, Guo J et al (2019) Modeling of heterogeneous reservoirs with damaged hydraulic fractures. *J Hydrol* 574:774–793. <https://doi.org/10.1016/j.jhydrol.2019.04.089>
- Zerzar A, Bettam Y (2003) Interpretation of multiple hydraulically fractured horizontal wells in closed systems. In: SPE international improved oil recovery conference in Asia Pacific <https://doi.org/10.2118/84888-MS>
- Zhang Y, Yang D (2021) Evaluation of transient pressure responses of a hydraulically fractured horizontal well in a tight reservoir with an arbitrary shape by considering stress-sensitive effect. *J Pet Sci Eng* 202:108518. <https://doi.org/10.1016/j.petrol.2021.108518>
- Zhao YL, Zhang LH, Luo JX et al (2014) Performance of fractured horizontal well with simulated reservoir volume in unconventional gas reservoir. *J Hydrol* 512:447–456. <https://doi.org/10.1016/j.jhydrol.2014.03.026>
- Zhao YL, Zhang LH, Shan BC (2018) Mathematical model of fractured horizontal well in shale gas reservoir with rectangular stimulated reservoir volume. *J Nat Gas Sci Eng* 59:67–79. <https://doi.org/10.1016/j.jngse.2018.08.018>
- Zhao G (2012) A simplified engineering model integrated stimulated reservoir volume (SRV) and tight formation characterization with multistage fractured horizontal wells. In: SPE Canadian unconventional resources conference <https://doi.org/10.2118/162806-MS>
- Zhou W, Banerjee R, Poe BD et al (2014) Semianalytical production simulation of complex hydraulic-fracture networks. *SPE J* 19(01):06–18. <https://doi.org/10.2118/157367-PA>

**Publisher's Note** Springer Nature remains neutral with regard to jurisdictional claims in published maps and institutional affiliations.